ESTROGEN IMPACTS NOD2-DEPENDENT REGULATION OF INTESTINAL HOMEOSTASIS

Mckenna Eklund[1], and Edan Foley[1, 2]

[1]Department of Medical Microbiology and Immunology, Faculty of Medicine and Dentistry, University of Alberta, Edmonton, AB, Canada.
[2]Department of Cell Biology, Faculty of Medicine and Dentistry, University of Alberta, Edmonton, AB, Canada.
Corresponding author: efoley@ualberta.ca.

ABSTRACT

Mutations in the innate immune receptor NOD2 are the greatest single genetic risk factors for Crohn's disease, yet the mechanisms by which NOD2 regulates intestinal homeostasis remain unclear. Here, we used a CRISPR-generated zebrafish model to determine the impacts of NOD2 deficiency on intestinal health. In a series of cellular, molecular, and transcriptomic studies, we uncovered substantial effects of NOD2 deficiency on epithelial and immune compartments, including deregulated expression of developmental pathways critical for establishment and maintenance of the gut epithelium, and an unexpected increase in the expression of multiple estrogen-response genes. In a series of functional assays, we uncovered a mechanistic link between estrogenic signals and NOD2-deficiency phenotypes, whereby exposure to estrogen alone replicated NOD2-deficiency phenotypes, and exposure to an estrogen receptor antagonist reverted the epithelial defects observed in NOD2 mutants. Our findings identify a critical NOD2-estrogen regulatory axis in the establishment of intestinal homeostasis and suggest that hormonal signaling may contribute to the sex-specific pathogenesis of Crohn's disease.

INTRODUCTION

Crohn's disease (CD) is a chronic inflammatory disorder of the gastrointestinal tract with significant public health implications [1]. The prevalence and incidence of CD continues to rise in North America and Europe, with particularly notable increases observed in developed and urbanized regions [1-3]. Mutations in the Nucleotide-binding Oligomerization Domain containing 2 (NOD2) locus are the most significant genetic risk factor for CD [4-9], increasing disease susceptibility by 15-40-fold and contributing to heightened risk of colorectal cancer [10,11].

Early studies proposed that NOD2 functions in Paneth cells to regulate antimicrobial peptide production, particularly α-defensins [12-17], in response to muramyl dipeptide (MDP) derived from bacterial peptidoglycan [18,19]. However, follow-up investigations suggested that defensin loss may be a consequence, rather than a cause, of CD, prompting a broader reevaluation of NOD2's function beyond antimicrobial defense [20-22]. Emerging evidence indicates that NOD2 plays a key role in regulating intestinal stem cell (ISC) function, particularly under stress conditions [23]. ISCs express high levels of NOD2 [24], and NOD2 is essential for stem cell proliferation in mouse models of T cell-induced enteropathy [25]. Additionally, NOD2 is essential for microbe-induced epithelial regeneration in malnourished models [26]. Despite these insights, it is unclear if NOD2 supports ISC function and epithelial renewal under steady-state conditions.

To investigate how NOD2 regulates intestinal homeostasis, we used zebrafish (*Danio rerio*), a well-established and genetically tractable model of human intestinal biology and disease [27-29]. Zebrafish and mammalian intestines share conserved immune and developmental pathways [30-41], including key components of NOD2 signaling [42]. Importantly, zebrafish offer unique advantages for examining epithelial interactions *in vivo*: their optical transparency enables live imaging of intestinal architecture. Additionally, zebrafish replicate pharmacologically actionable CD phenotypes [43] and allow for high-throughput manipulation using CRISPR-based genome editing [44,45].

In this study, we combined single-cell RNA sequencing, targeted gene expression analysis, and *in vivo* functional assays to investigate NOD2 regulation of intestinal epithelial proliferation, differentiation, and cell survival under homeostatic conditions. We uncovered a NOD2-estrogen

signaling axis that is critical for intestinal homeostasis *in vivo*. These findings provide new insights into the cellular mechanisms underlying NOD2-associated intestinal dysfunction and may help explain sex-specific variation in disease susceptibility, offering a novel perspective on CD pathogenesis.

RESULTS

NOD2 deficiency reduces intestinal length but does not alter microbiota composition in zebrafish.

To investigate the role of NOD2 in intestinal homeostasis, we used CRISPR-Cas9 mutagenesis to generate *nod2* mutant zebrafish that harbor a 4-base pair deletion in the first coding exon, resulting in a frameshift and premature stop codon that produces a severely truncated, non-functional NOD2 protein (Fig 1A). Despite this loss of function, *nod2*$^{-/-}$ zebrafish are homozygous viable, with no significant change in body weight (Fig 1B), but a 20% reduction in total gut length compared to WT controls (Fig 1C). To test whether NOD2 deficiency alters microbiome composition in zebrafish, we sequenced the V4 region of the 16S rRNA gene from adult co-housed WT and *nod2*$^{-/-}$ siblings. Rarefaction curves confirmed sufficient sequencing depth (Fig 1D). Consistent with previous work [21], we found that NOD2 deficiency did not cause major shifts in microbial composition under homeostatic conditions (Fig 1E-H). These results indicate that *nod2*-deficiency in zebrafish reduces intestinal length without altering the composition of intestinal bacterial communities, indicating that fish represent a robust and accessible model for examining homeostatic roles of NOD2.

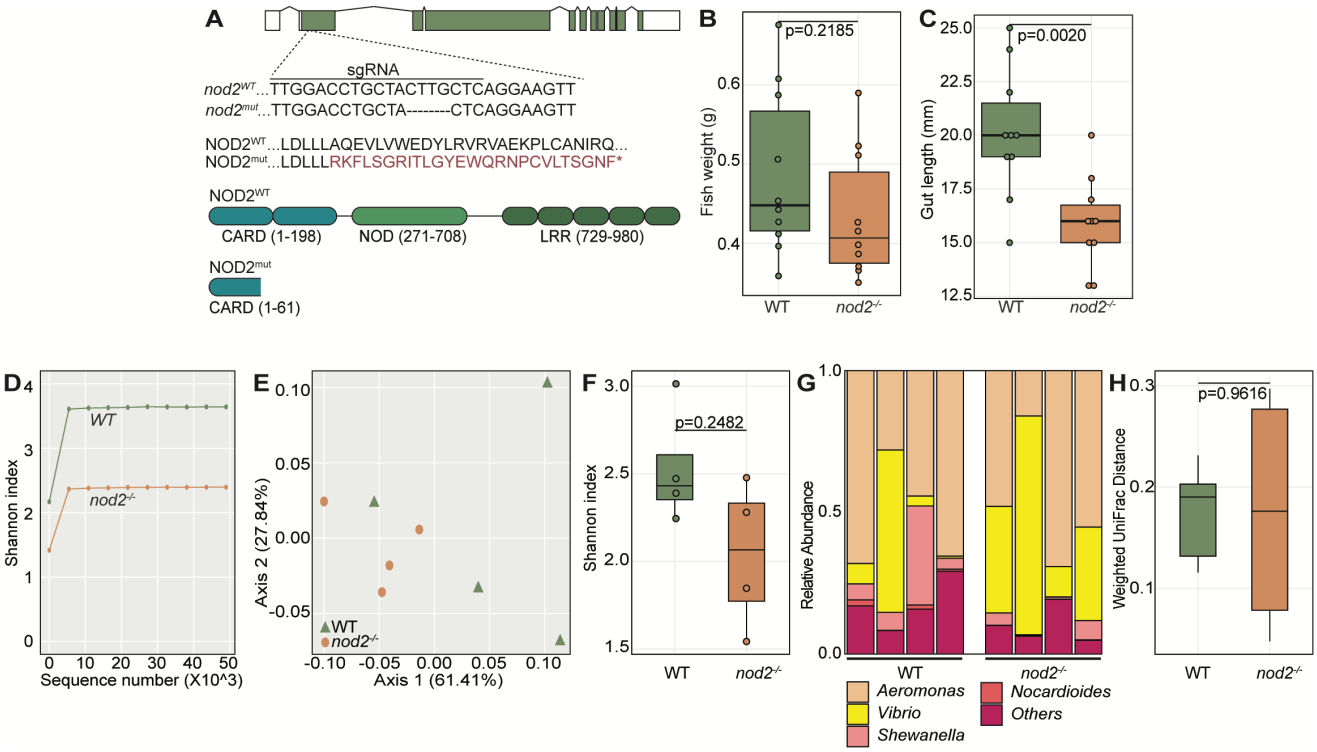

Fig 1. Generation of a nod2-deficient zebrafish model reveals reduced gut length without major microbiome disruption. A) Schematic map of *nod2* protein coding gene transcript structure with all introns and exons (coding DNA in green). A sgRNA targeting exon 2 of nod2, within the region encoding the first CARD domain, was used to generate a 4-base pair deletion via CRISPR-Cas9. Measurements of **B)** fish weight and **C)** gut length in WT and *nod2*$^{-/-}$ zebrafish in-crossed siblings; *nod2*$^{-/-}$ zebrafish exhibit significantly shorter gut lengths compared to WT, while body weight is comparable. **D)** Rarefaction curves and **E)** PCoA plot of Shannon Index score and the Weighted UniFrac Distance of co-housed WT and *nod2*$^{-/-}$ zebrafish groups as a measure of alpha- and beta-diversity, respectively. **F)** Boxplots pertaining to the Shannon Index Score of each genotype as a measure of alpha-diversity. **G)** Relative abundance bar plot of the bacterial genera in co-housed WT and *nod2*$^{-/-}$ zebrafish intestines. Each bar represents a single intestine. **H)** Boxplots pertaining to the Weighted UniFrac Distance of each genotype as a measure of beta-diversity. P-values were calculated using Mann-Whitney U test.

High-resolution profiling of NOD2-deficient intestines uncovers early immune and epithelial alterations

To determine how NOD2 deficiency impacts gut homeostasis, we performed single-cell RNA sequencing on whole intestines from co-housed, in-crossed WT and *nod2*$^{-/-}$ siblings (2 males and 3 females per group), effectively minimizing artefactual impacts of environmental and genetic variability. As zebrafish intestines include most cell types found in mammalian intestines [30,31,37], this approach allowed us to characterize the consequences of NOD2 deficiency for all major intestinal cell types. In total, we generated high-quality transcriptomic data for 11,490 cells, that resolved into 13 distinct transcriptional clusters (Fig 2A, B) based on established markers from both zebrafish [30,31] and mammalian gut studies [37,46].

Gene ontology analysis revealed widespread transcriptional changes in *nod2*$^{-/-}$ intestines, with impacts on processes related to growth, development, and survival across epithelial and immune compartments, as well as modest shifts in cell type proportions, including apparent loss of goblet cells and increase in leukocyte numbers (Fig 2C, D).

Given the central role of gut-associated leukocytes in CD [47,48] and the high expression of NOD2 in intestinal immune cells [49-53], we elected to characterize effects of NOD2 deficiency on leukocyte transcriptional states in greater detail (Fig 2E-H). Gut-associated leukocytes were identified based on transcriptional clustering and canonical immune marker gene expression (Fig S1). We discovered notable impacts of NOD2 deficiency on gut-associated leukocytes, including altered

expression of co-stimulatory and cytotoxic markers in T cells (Fig 2E); reduced expression of *il22* and *il7r* in ILC3s (Fig 2F); and dysregulated NF-κB signaling in granulocytes (Fig 2H). In macrophages, CD-linked *cxcl8b.1* was downregulated, while fibrosis and autophagy associated genes (*cd9a*, *atg4c*) were upregulated (Fig 2G). Additionally, *nod2*$^{-/-}$ IECs exhibit altered expression of chemokines (e.g., *cxcl8a.6, ccl20b, cxcr3.1*) and cytokine signaling components (e.g., *il2rga*, *il17rc*, *il34*, Fig S1A-B), while stromal cells altered transcripts related to leukocyte activation and adhesion (e.g., *cd74a*, *cd248a,* Fig S1A-B), indicating significant shifts in the immune landscape of NOD2-deficient adults.

To evaluate the *in vivo* consequences of these transcriptional shifts, we used immunohistochemistry to quantify the abundance of cells that express the pan-leukocyte Lcp1 marker in aged NOD2-deficient guts and wildtype controls (Fig 2I, J). Consistent with the widespread impacts of NOD2 deficiency on leukocyte transcriptional states, we observed a significant accumulation of Lcp1^{+} cells in aged *nod2*$^{-/-}$ intestines relative to wildtype controls (Fig 2K), confirming that NOD2-deficienct intestines harbor a larger population of functionally dysregulated immune cells.

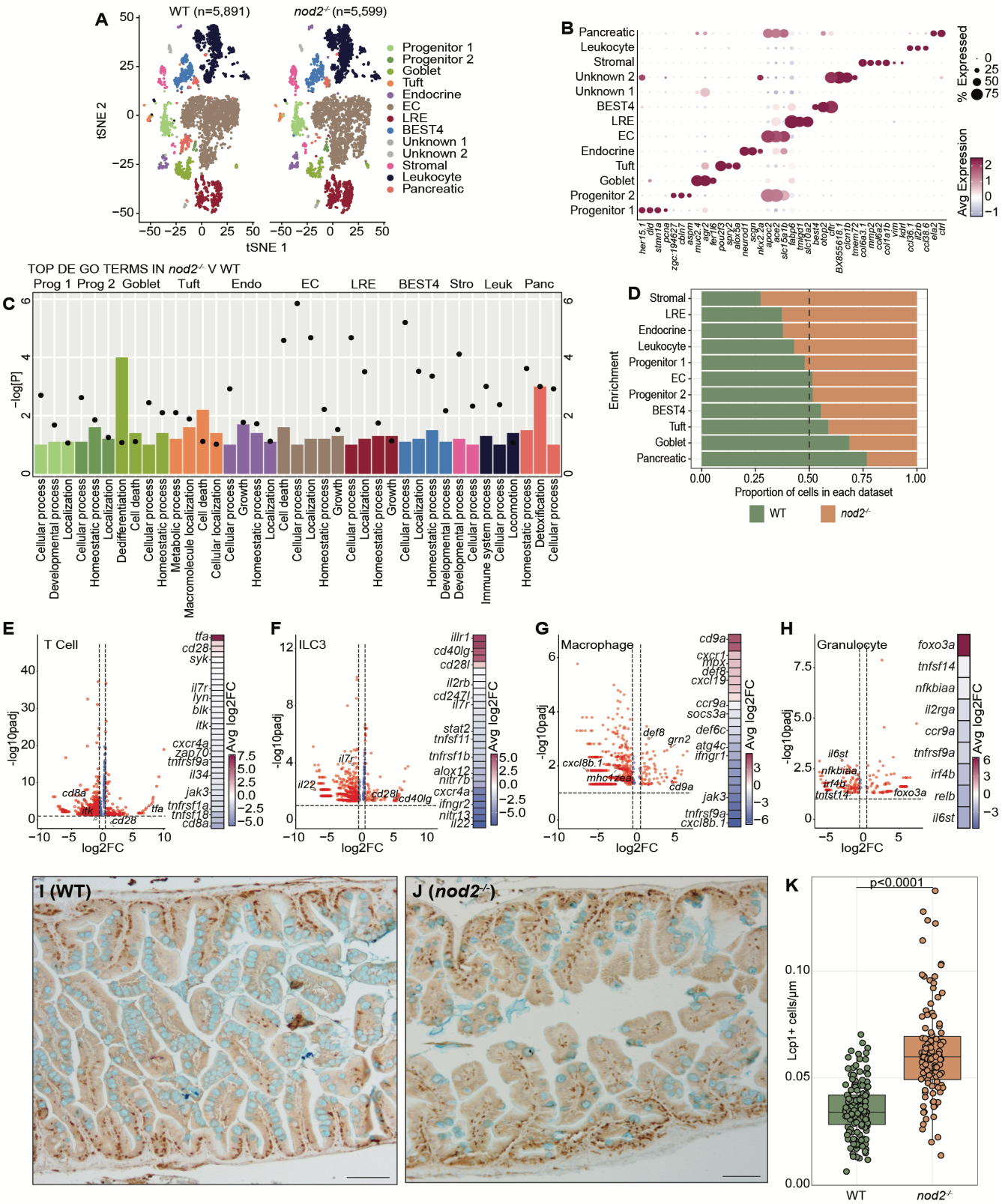

Fig 2. NOD2 deficiency alters intestinal epithelial and immune cell transcriptional programs. A) Individual 2D t-distributed stochastic neighbor embedding (tSNE) projections of 11,490 intestinal cells color coded by cell type, including progenitors, absorptive enterocytes (ECs), lysosome-rich enterocytes (LREs), goblet cells, tuft cells, stromal cells, and others. **B)** Dotplot representation of the expression

levels of established markers in the indicated cell types. **C)** Representation of the top gene ontology terms associated with DE genes in *nod2*$^{-/-}$ intestines relative to WT sibling controls for each cell type. Relative enrichment score for each term is indicated by bar length and the negative log p-values are shown with closed circles. **D)** Bar plot displaying the proportional representation of each cell type in WT and *nod2*$^{-/-}$ datasets and log-scale quantification of cells per cluster. **E-H)** Volcano plots of DE genes in *nod2*$^{-/-}$ intestines relative to WT sibling controls in the indicated cell type (genes upregulated in *nod2*$^{-/-}$ appear on the right; downregulated genes appear on the left). Only genes with absolute $\log_2$ fold change greater than 0.25 and adjusted p-value ≤ 0.05 are shown. Select significantly dysregulated genes are labeled. Heatmaps display scaled expression values of top immune-related genes across each cell type. **I-J)** Immunohistochemical staining and **K)** quantification of Lymphocyte Cytosolic Protein 1 (Lcp1)$^{+}$ cells per µm in co-housed 18-month-old (aged) WT and *nod2*$^{-/-}$ intestines. n = 5 fish per group; each point represents an individual measurement obtained from multiple images per fish intestine. Scale bars = 100µm. P-values were calculated using Mann-Whitney U test.

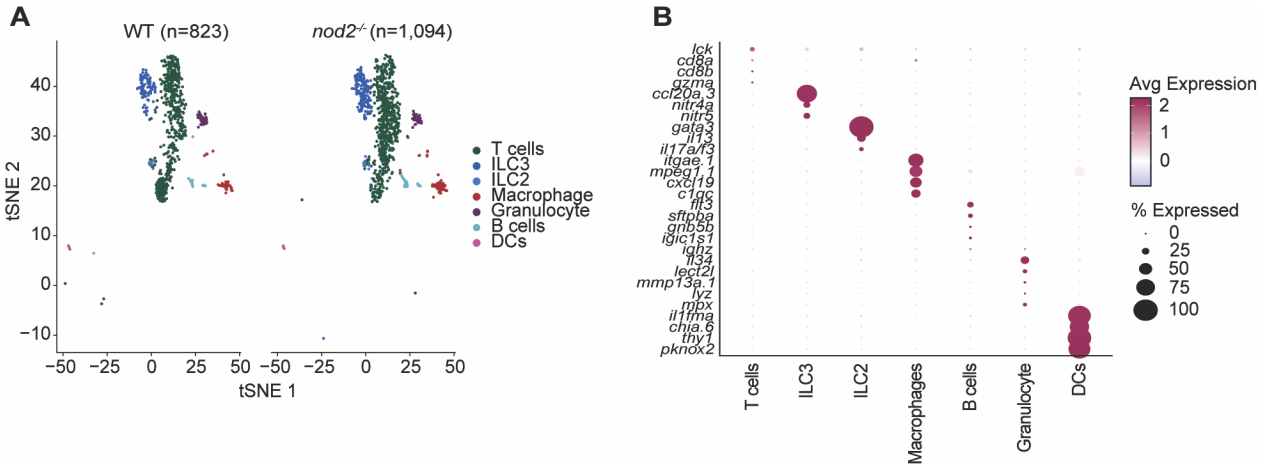

Supplementary Fig 1. Identification of intestinal immune cell populations in WT and *nod2*$^{-/-}$ intestines. A) tSNE visualization of leukocytes isolated from WT (left) and *nod2*$^{-/-}$ (right) zebrafish intestines, colored by immune cell type based on transcriptional clustering and marker gene expression. Major immune subsets identified include T cells, ILC3s, ILC2s, macrophages, granulocytes, B cells, and dendritic cells (DCs). **B)** Dotplot representation of the expression levels of established markers in the indicated cell types from integrated data set.

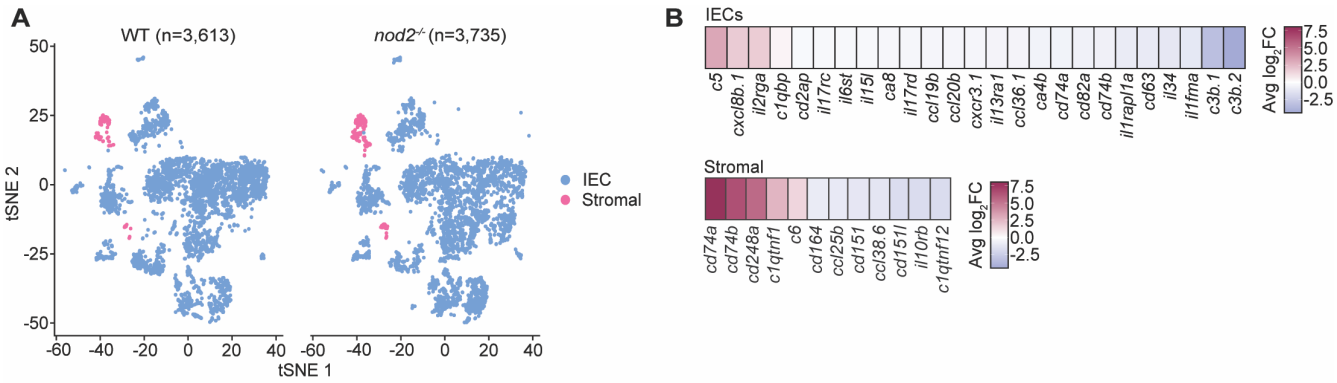

Supplementary Fig 2. NOD2 deficiency enhances leukocyte-recruitment gene signatures in epithelial and stromal compartments. A) tSNE plots of intestinal epithelial cells (IECs; blue) and stromal cells (pink) from WT and *nod2*$^{-/-}$ zebrafish. **B)** Heatmaps showing differential expression of immune cell recruitment-associated genes in IECs and stromal cells (adjusted p-value ≤ 0.05).

NOD2 regulates intestinal epithelial progenitor dynamics

Alongside anticipated effects on immune-regulatory leukocytes, we noted dysregulated gene expression in NOD2-deficienct epithelial lineages, including genetic pathways linked to cell growth, development and survival (Fig 2C). Given the central role of the intestinal epithelium as a barrier to microbial invasion, we investigated whether NOD2 is required for epithelial renewal. To evaluate this, we focused on cellular features associated with tissue replenishment, starting with progenitor cell proliferation. Using our single-cell RNA sequencing data, we found that NOD2 deficiency significantly attenuated the expression of key growth regulators in the progenitor cell populations (Fig 3A), including critical elements of the Wnt/β-catenin (*wnt7ba*), TGFβ (*tgif1*), and growth (*myca*) pathways (Fig 3B), suggesting that NOD2-deficiency disrupts the molecular framework required for intestinal epithelial growth and renewal. Feature plots confirmed expression within progenitor populations, supporting their relevance to early epithelial renewal programs (Fig 3C, D).

To test putative roles for NOD2 in epithelial cell proliferation, we quantified incorporation of the S phase marker EdU in intestines of WT and *nod2*$^{-/-}$ larvae raised under conventional conditions. We discovered that NOD2 deficiency led to a 50% drop in the number of cycling cells (Fig S3A, B), confirming that NOD2 is required to sustain progenitor proliferation *in vivo*. To determine whether this effect depends on microbial cues, we repeated the EdU labeling assay with axenic larvae alongside a conventionally reared control population. In agreement with a previous study [41], we found that wildtype fish exhibited reduced proliferation under axenic conditions (Fig. 3F, G), confirming that gut microbes promote epithelial proliferation. Consistent with data in Fig. S3, we observed a near 50% decline of EdU incorporation in conventionally reared *nod2*$^{-/-}$ intestines relative to their wildtype counterparts. However, proliferation rates were equivalent between both genotypes in the absence of microbes (Fig 3F-G), suggesting that NOD2 promotes epithelial proliferation in response to bacterial cues.

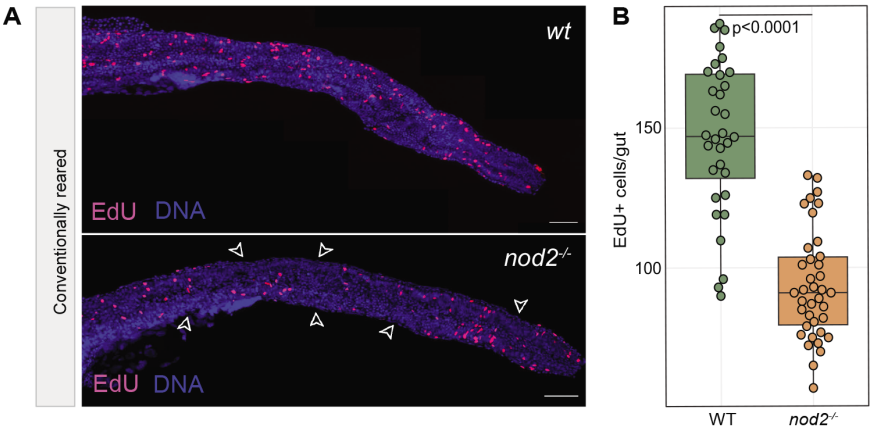

Supplementary Fig 3. NOD2 is required for epithelial proliferation in the developing zebrafish gut. A) Immunofluorescent images of whole-mount intestines from conventionally reared WT and *nod2*$^{-/-}$ larvae. EdU^{+} cells (magenta) and nuclei (blue, DNA) are shown in merged false-colored images. White arrowheads highlight regions where *nod2*$^{-/-}$ intestines lacking EdU^{+} cells. Scale bars= 150µm. **B)** Quantification of total EdU^{+} cells per gut in WT and *nod2*$^{-/-}$ larvae. Each point represents an individual larva; *nod2*$^{-/-}$ intestines exhibit a significant reduction in proliferating cells. P-values were calculated using Mann-Whitney U test.

To directly test if the canonical NOD2 ligand, MDP, is sufficient to induce intestinal epithelial proliferation, we used flow cytometry to quantified cycling cells in intestines of axenic WT and NOD2-deficient larvae that we treated with MDP. We found that MDP treatment more than doubled the number of EdU^{+} cells in WT larvae, establishing it as a potent microbial cue for intestinal growth (Fig 3H). In contrast, the pro-growth effect of MDP was substantially impaired in *nod2*$^{-/-}$ larvae with only a minor increase in EdU^{+} cells, demonstrating that the MDP-NOD2 axis links microbial sensing to intestinal stem cell proliferation.

We then assessed proliferation in WT and NOD2-deficient adults using PCNA labeling, which marks cells in S phase of the cell cycle. Here, we once more observed a significant reduction in proliferative PCNA^{+} cells in the intestines of NOD2-deficient adults relative to WT controls (Fig 3I, J), Together, our results establish NOD2 as a regulator of epithelial renewal, linking microbial recognition to epithelial cell proliferation during developmental and adult life stages, and demonstrating an essential role for NOD2 in intestinal growth and homeostasis.

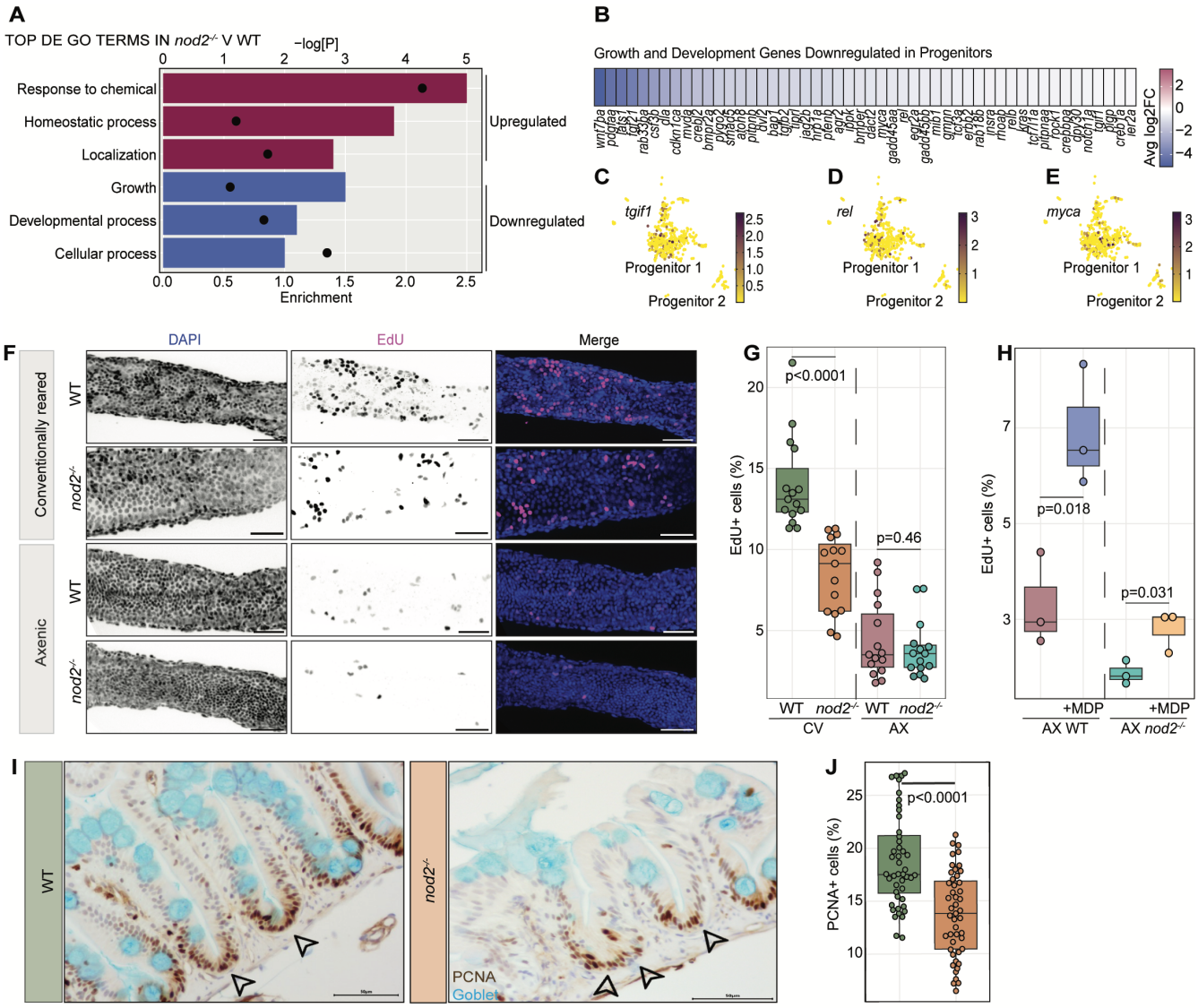

Fig 3. *nod2*-deficiency impairs intestinal growth and proliferation. A) The top three up, or downregulated gene ontology terms in *nod2*$^{-/-}$ progenitor cells relative to WT controls. Relative enrichment score for each term is indicated by bar length and the negative log p-values are shown with closed circles. **B)** Heatmap of representative growth and development gene expression in *nod2*$^{-/-}$ progenitor cells relative to WT controls (adjusted p-value ≤ 0.05). **C-E)** Feature plots showing the expression of *tgif1* (C), *rel* (D), and *myca* (E) of WT or *nod2*$^{-/-}$ integrated dataset. **F)** Immunofluorescence images of conventionally reared or germ-free WT or *nod2*$^{-/-}$ larval intestines. In merged false-colored images, DNA is labeled in blue and EdU^{+} cells in magenta. Scale bars = 35µm. **G)** Quantification of the percentage of EdU^{+} cells in conventionally reared or germ-free WT or *nod2*$^{-/-}$ larval intestines. Each dot represents a measurement from a single fish intestine. **H)** Flow cytometry quantification of the percentage of EdU^{+} cells in germ free WT or *nod2*$^{-/-}$ larval intestines. Larvae were mock or MDP-treated (1µg/ml). One dot represents 15 zebrafish larvae guts. **I)** Immunohistochemical images of a sagittal posterior intestine section from WT and *nod2*$^{-/-}$ intestines stained with primary antibody for Proliferating cell nuclear antigen (PCNA- arrowheads). Sections were counterstained in Alcian blue (Goblet) and quarter-strength Hematoxylin Gill III. Scale bars are indicated in each panel. **J)** Quantification of % PCNA^{+} cells from multiple sections of WT and *nod2*$^{-/-}$ intestines. Each dot represents a single villus

measurement from multiple zebrafish intestines. Scale bars = 100μm. P-values were calculated using Mann-Whitney U test or Kruskal-Wallis test.

Loss of NOD2 disrupts epithelial homeostasis by altering cell death and differentiation

While NOD2 is well established as a microbial sensor, its role epithelial cell dynamics *in vivo* remains poorly understood. Our transcriptomic analysis showed that NOD2 deficiency alters the expression of genes involved in proliferation and cell death across all major secretory epithelial lineages, including goblet cells, enteroendocrine cells, and tuft cells (Fig 2D,4A). As NOD2 dysfunction can impair secretory cell function [54], we determined if NOD2 is required for epithelial cell composition and survival. To characterize the impact of NOD2 loss on epithelial cell survival and identity in the intestinal epithelial barrier, we used TUNEL and Anxa4 staining to quantify apoptotic and secretory cell populations in co-housed WT and *nod2*$^{-/-}$ in-crossed siblings (Fig 4B-D). We found that *nod2* mutants had a significant increase in TUNEL^{+} cells and a loss of Anxa4^{+} secretory cells (marked by 2F11) relative to WT controls (Fig 4B-D), indicating elevated apoptosis and loss of secretory cell populations in NOD2-deficient guts.

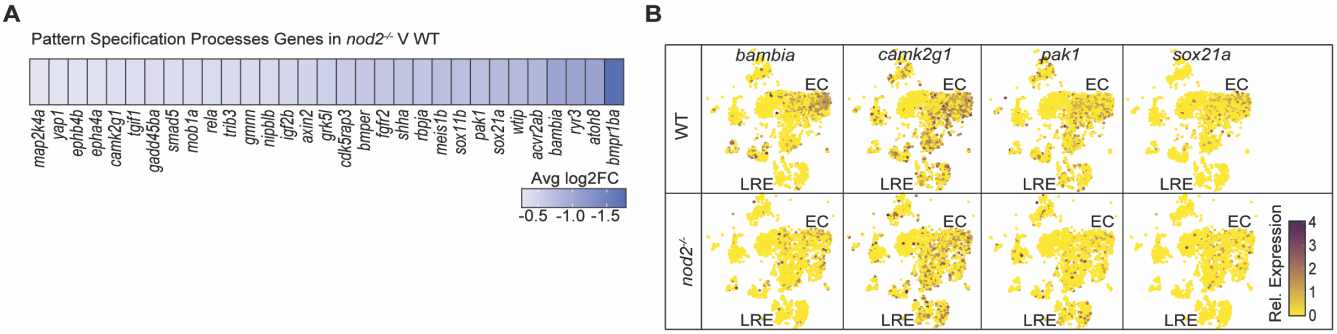

Supplementary Fig 4. Loss of NOD2 impairs expression of pattern specification genes in the intestinal epithelium. A) Heatmap illustration of representative pattern specification processes gene expression in *nod2*$^{-/-}$ versus WT adult intestinal epithelium (adjusted p-value ≤ 0.05). **B)** Feature plots showing relative expression of select patterning genes (*bambia*, *camk2g1*, *pak1*, *sox21a*) in WT and *nod2*$^{-/-}$ intestinal epithelium. Expression is reduced across enterocyte (EC) and lower right epithelial (LRE) clusters in *nod2*$^{-/-}$ intestines, indicating broad loss of epithelial patterning cues.

Beyond cell survival, epithelial architecture depends on precise transcriptional patterning programs that establish the cellular heterogeneity required for a fully functional intestinal epithelium. Our differential gene expression analysis uncovered downregulation of key patterning genes in *nod2*$^{-/-}$

intestines, including *map2k4a*, *epb41l4b*, *camk2g1*, *pak1*, and *sox21a* (Fig S4A, B), suggesting that NOD2 modifies genetic programs that regulate spatial identity and cell fate. To test possible roles for NOD2 in epithelial patterning, we quantified Anxa4^{+} secretory cells in the intestines of WT and *nod2*$^{-/-}$ larvae raised under either conventional or axenic conditions. Under conventional conditions, *nod2*$^{-/-}$ larvae exhibited a significant reduction in Anxa4^{+} cells compared to WT siblings (Fig 4E, F). This reduction was not observed in axenic *nod2*$^{-/-}$ larvae, suggesting that commensal microbes typically engage NOD2 to promote maturation of secretory lineages in the gut. Supporting this, we discovered that *nod2*$^{-/-}$ intestines also exhibited shorter villi and fewer goblet cells (Fig 4G, H), reflecting impaired secretory lineage differentiation, and mirroring patient data [55,56] that associate NOD2 mutations with goblet cell loss.

To assess the impact of NOD2 deficiency on goblet cell function, we performed whole-mount Alcian blue staining of intestinal mucus in wildtype and nod2 mutant larvae. We found that *nod2* mutants displayed a significant reduction in Alcian blue^{+} area under homeostatic conditions (Fig 4I, J), indicating reduced goblet cell function. Treatment with dextran sulfate sodium (DSS), a sulfated polysaccharide that induces epithelial damage and inflammation in vertebrate models, led to an expansion of the mucus barrier in both genotypes, with Alcian blue^{+} area approximately doubling in each. While the relative increase was similar, the absolute barrier size remained lower in *nod2*$^{-/-}$ larvae, suggesting that epithelial stress can partially rescue goblet cell function through NOD2-independent mechanisms, though the response remains blunted in the absence of NOD2.

Combined, our observations point to a critical role for NOD2 in maintaining epithelial homeostasis, but raise a key mechanistic question: what is the underlying genetic driver that contributes to the epithelial phenotypes observed in *nod2*$^{-/-}$ mutants?

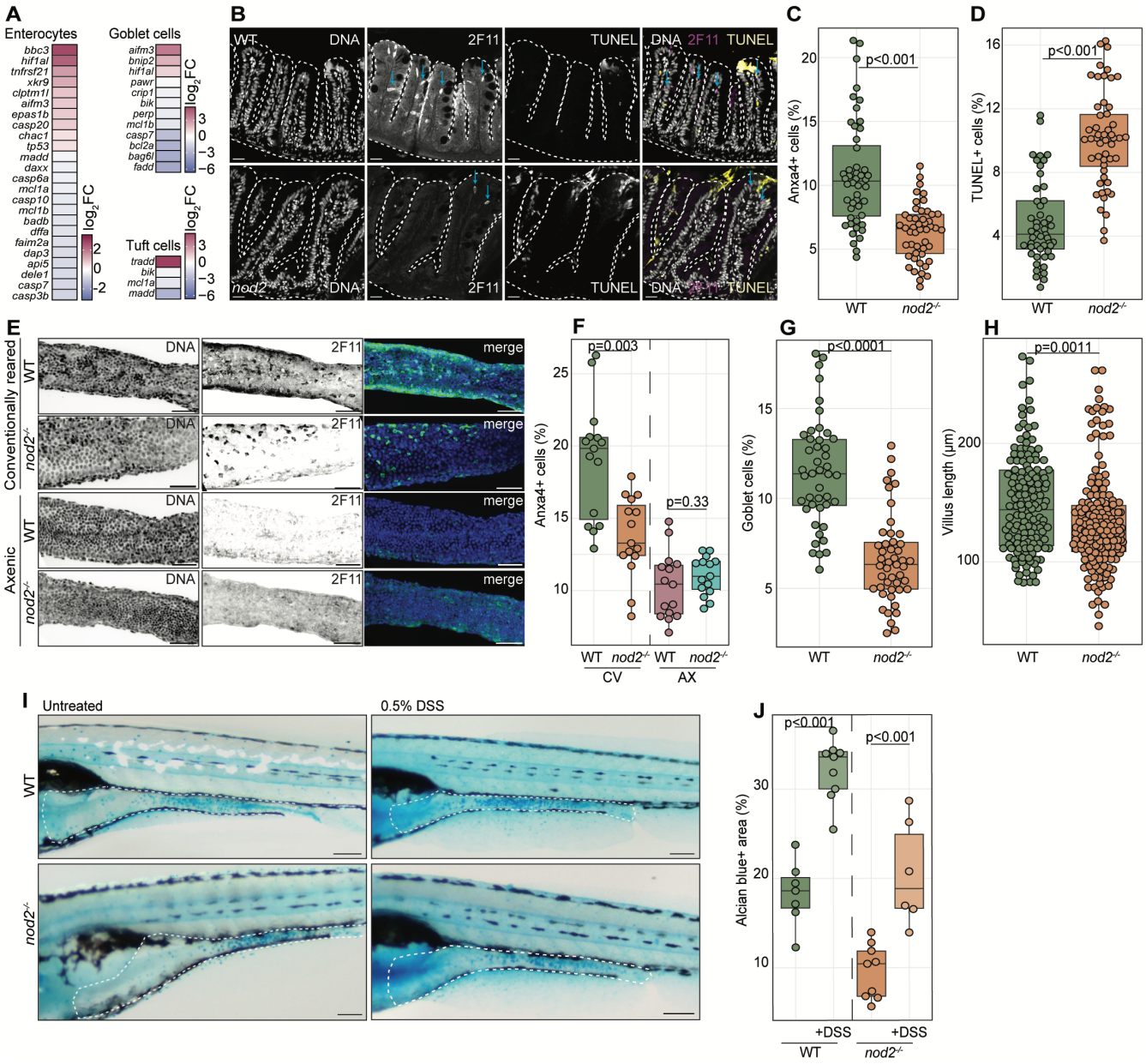

Fig 4. Loss of *nod2* disrupts epithelial homeostasis by altering cell death and cell fate. A) Heatmap of cell death gene expression in *nod2*$^{-/-}$ ECs, goblet cells, and tuft cells relative to WT controls (adjusted p-value ≤ 0.05). **B-D)** Quantification of % Anxa4^{+} cells (C) (blue arrows), and % TUNEL^{+} cells (D) from multiple sections of WT and *nod2*$^{-/-}$ intestines. Each dot represents a single villus measurement from multiple zebrafish intestines. **E)** Immunofluorescent images of conventionally reared or axenic WT or *nod2*$^{-/-}$ larval intestines. In merged false-colored images, DNA is labeled in blue and Anxa4^{+} cells in green. Scale bars = 35µm. **F)** Quantification of the percentage of Anxa4^{+} cells. Each dot represents a measurement from a single fish intestine. **G-H)** Quantification of % Alcian-blue+ (goblet cells) (G) and villus length (H) and from multiple sections of WT and *nod2*$^{-/-}$ intestines. Each dot represents a single villus measurement from multiple zebrafish intestines. **I-J)** Alcian blue staining (I) and quantification of Alcian blue^{+} area (J) in WT, *nod2*$^{-/-}$, WT+DSS, and *nod2*$^{-/-}$+DSS whole mount larvae. Scale bars = 150 µm. P-values were calculated using Mann-Whitney U test or Kruskal-Wallis test.

NOD2 deficiency enhances estrogen signaling in the intestinal epithelium

To investigate the molecular pathways responsible for epithelial disruption in *nod2*$^{-/-}$ intestines, we examined our transcriptomic data for signatures of impaired signaling in NOD2-deficient adult intestines and identified enrichment of estrogen response pathways as the most prominently affected (Fig 5A-B). The zebrafish genome encodes *esr1*, and *esr2*, orthologs of ERα and ERβ, respectively. A subsequent genome duplication event led to evolution of *esr2a* and *esr2b* paralogs from the ancestral *esr2* gene [57]. We discovered enriched expression of *esr2b* specifically in IECs (Fig 5C) and found that NOD2-deficiency led to marked upregulation of many estrogen-response genes, including vitellogenins (*vtg1*-*vtg7*) and *esr2b* in multiple epithelial cell types (Fig 5-E), indicating elevated estrogen signaling in NOD2-deficient guts. To validate the estrogen-related transcriptional changes observed in our scRNA-seq data, we performed qPCR for *vtg1*, *vtg2*, and *vtg4* in WT and *nod2*$^{-/-}$ adult zebrafish intestines, separated by sex (Fig 5F, G). We found that, in males, *vtg1*, *vtg2* and *vtg4* levels remained unchanged between WT and *nod2*$^{-/-}$ (Fig 5F). In contrast, *nod2*$^{-/-}$ females exhibited significant increases in *vtg* gene expression compared to WT controls (Fig 5G), confirming that NOD2 deficiency enhances estrogen-responsive gene expression in a sex-specific manner.

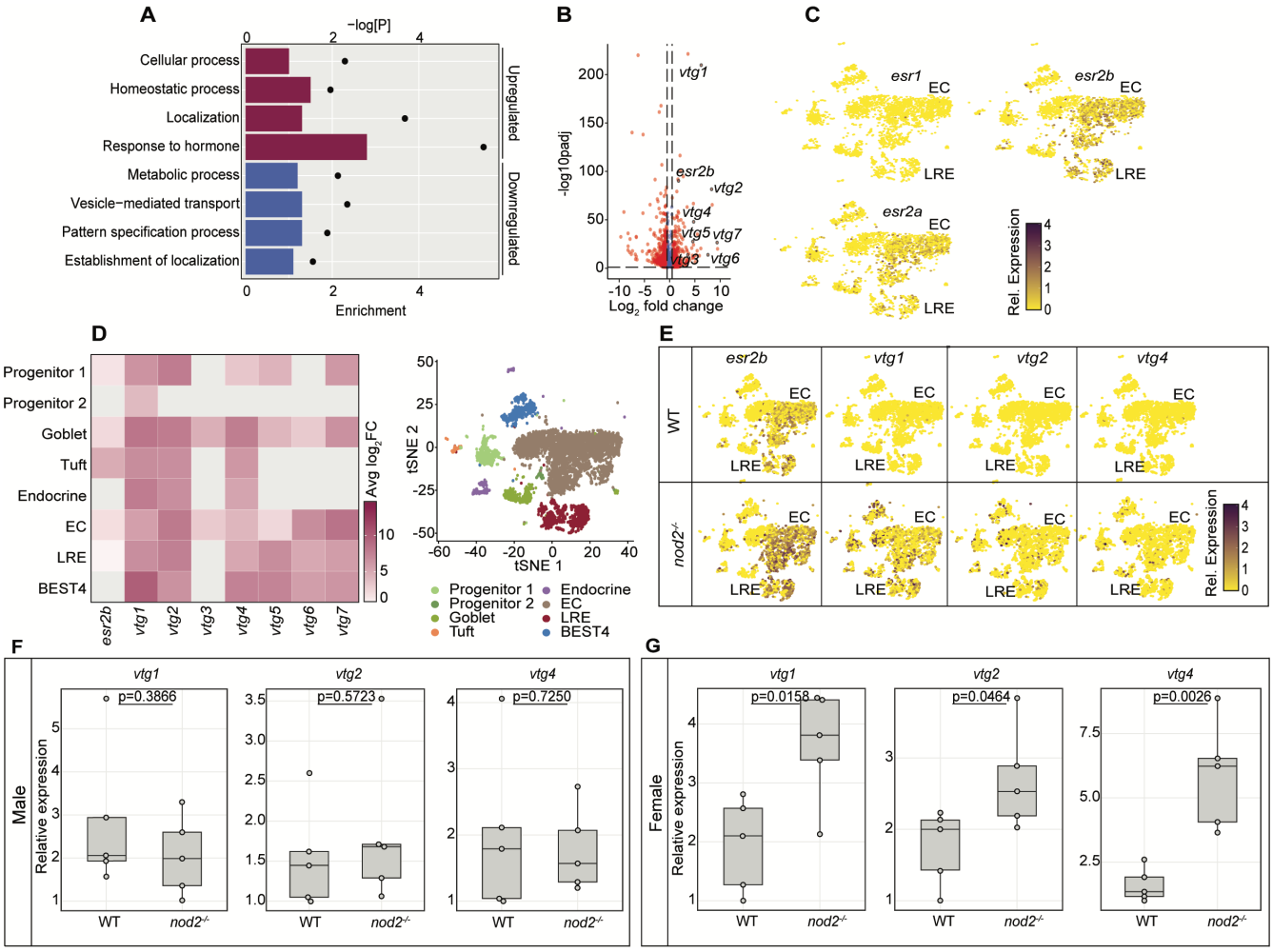

Fig 5. NOD2-deficiency significantly increased the intestinal estrogen response. **A)** The top four up, or downregulated gene ontology terms in *nod2*$^{-/-}$ epithelium relative to WT controls. Relative enrichment score for each term is indicated by bar length and the negative log p-values are shown with closed circles. **B)** Volcano plot of integrated dataset DE genes in *nod2*$^{-/-}$ epithelium relative to WT controls. Significance values represented on the y-axis and relative fold change of gene expression on the x axis. Only genes with log2 expression changes greater than 0.25 are shown. Genes listed as response to hormone are indicated. **C)** Feature plots showing relative expression of the estrogen receptors *esr1*, *esr2a*, and *esr2b* in intestines of WT fish. Enterocytes (EC) and Lysosome-Rich Enterocytes (LRE) are labeled for orientation. **D)** Heatmap (left) showing relative changes in expression of estrogen response genes, including *esr2b* in NOD2-deficient fish relative to WT counterparts (adjusted p-value ≤ 0.05), and tSNE plot (right) showing epithelial cell type annotations. **E)** Feature plots showing expression of *esr2b*, *vtg1*, *vtg2*, and *vtg4* in WT and *nod2*$^{-/-}$ datasets. **F-G)** qPCR analysis of vitellogenin genes (*vtg1*, *vtg2*, and *vtg4*) in WT and *nod2*$^{-/-}$ adult zebrafish intestines, separated by sex. P-values were calculated using Mann-Whitney U test or Kruskal-Wallis test.

Estrogen signaling modulates intestinal epithelial proliferation and goblet cell abundance through a NOD2-dependent mechanism

Given the established links between estrogen signaling and epithelial cell proliferation and survival [58-60], we asked if estrogen and NOD2 interact to control intestinal cell fates. To this end, we analyzed epithelial function in WT and NOD2-deficient larvae that we treated with 17β-estradiol (E2), or the estrogen receptor antagonist tamoxifen. As zebrafish larvae are estrogen-sensitive hermaphrodites [61-64], they provide a unique opportunity to examine sex-independent effects of estrogen on gut physiology. To test if interactions between estrogen and NOD2 modify intestinal renewal, we quantified intestinal epithelial proliferation in wildtype and *nod2*$^{-/-}$ larvae that we treated with 17β-estradiol (E2), or the vehicle control DMSO, for 24 hours. We discovered that E2 treatment reduced the number of proliferative cells by over 50% in wildtype larvae but had negligible impacts on proliferation in NOD2-deficient counterparts (Fig 6A, B). Notably, pre-treatment with the antiestrogen tamoxifen [65] had the opposing effect. Tamoxifen exposure significantly elevated intestinal proliferation rates in NOD2-deficient larvae without having any discernible impacts on wildtype controls (Fig 6C, D).

Looking at goblet cell function, we detected similar interactions between NOD2 and estrogen. Exposure to E2 significantly reduced the Alcian blue-positive area of wildtype larval intestines but had no effect on Alcian blue levels in *nod2*$^{-/-}$ intestines. (Fig 6E, F). In contrast, goblet cell numbers in NOD2-deficient intestines were unaffected by E2 exposure, suggesting that epithelial responses to estrogen are already maximally engaged in the absence of NOD2. Finally, we found that tamoxifen treatment nearly doubled the intestinal Alcian blue-positive area of *nod2*$^{-/-}$ intestines, with no discernible effects on WT siblings (Fig 6G, H). In sum, our work shows that treatment of wildtype larvae with E2 replicates the proliferative and barrier defects noted in NOD2-deficient larvae, while tamoxifen exposure partially rescues barrier defects in *nod2*$^{-/-}$ intestines, indicating a critical role for a NOD2-estrogen axis in the maintenance of intestinal epithelial homeostasis.

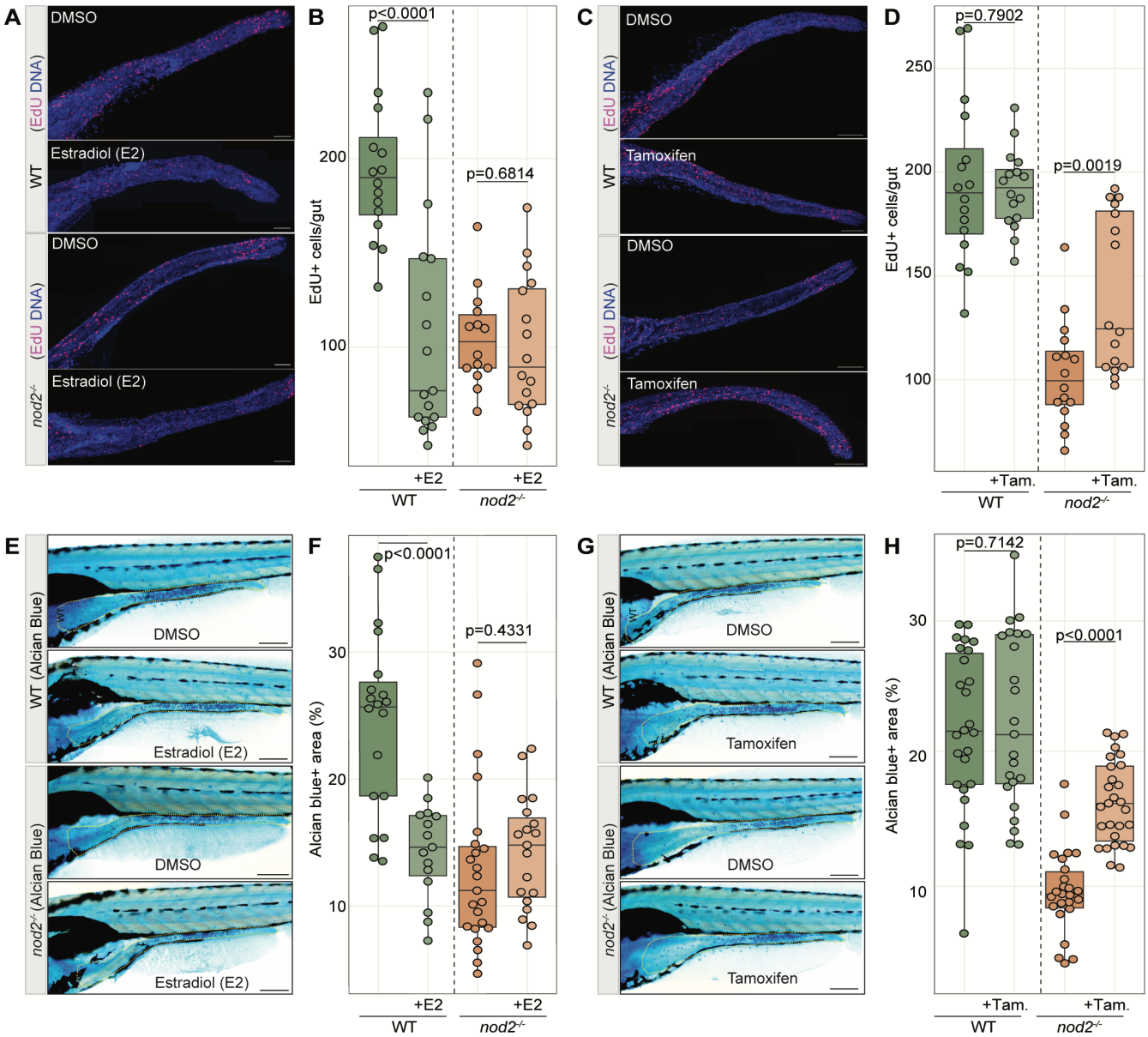

Fig 6. Intestinal epithelial proliferation and goblet cell abundance are regulated by NOD2-dependent estrogen signaling. A) Immunofluorescence of whole-mount WT and *nod2*$^{-/-}$ larval intestines treated with DMSO (vehicle control) or 25 ng/μL estradiol (E2). In merged false-colored images, DNA is labeled in blue and EdU^{+} proliferating cells in magenta. Scale bars = 150 μm. **B)** Quantification of EdU^{+} cells per gut. Each dot represents one fish. Estrogen significantly reduced proliferation in WT larvae but not in *nod2*$^{-/-}$. **C)** Immunofluorescence of WT and *nod2*$^{-/-}$ larval intestines treated with DMSO or 1.5 ng/μL Tamoxifen (Tam). DNA is labeled in blue and EdU+ cells in magenta. Scale bars = 150 μm. **D)** Quantification of EdU^{+} cells per gut. Tamoxifen increased proliferation in *nod2*$^{-/-}$ larvae but had no effect in WT. **E-F)** Alcian blue staining (E) and quantification of Alcian blue^{+} area (F) in WT and *nod2*$^{-/-}$ larvae treated with DMSO or E2. E2 significantly reduced goblet cell area in WT, but not in *nod2*$^{-/-}$ larvae. **G-H)** Alcian blue staining (G) and quantification (H) of goblet cell area in WT and *nod2*$^{-/-}$ larvae treated with DMSO or tamoxifen. Tamoxifen significantly increased goblet cell abundance in *nod2*$^{-/-}$ larvae. P-values were calculated using the Mann-Whitney U test.

Estrogen signaling impairs epithelial recovery in a NOD2-dependent manner

To assess the functional consequences of NOD2 deficiency during intestinal injury, we monitored survival rates of wildtype and NOD2-deficient larvae that we exposed to DSS. Kaplan-Meier survival analysis revealed a significant reduction in survival for *nod2*$^{-/-}$ larvae following DSS exposure compared to WT controls (Fig 7A), indicating that loss of NOD2 compromises the ability to withstand a pro-inflammatory epithelial injury. Given the transcriptional enrichment of estrogen signaling pathways in *nod2*$^{-/-}$ intestines, we next asked whether estrogen modulates intestinal resilience in a NOD2-dependent manner. To this end, we pretreated WT and *nod2*$^{-/-}$ larvae with E2 prior to a DSS challenge. As anticipated, we found that *nod2*$^{-/-}$ larvae exhibited poor survival regardless of E2 treatment status, and we found that wildtype larvae effectively survived an acute DSS challenge, confirming a role for NOD2 in regulating host responses to a pro-inflammatory challenge (Fig 7B). Strikingly, we discovered that E2-treated WT larvae phenocopied the heightened sensitivity observed in *nod2*$^{-/-}$ animals, confirming that estrogen impairs epithelial recovery in a NOD2-dependent mechanism (Fig 7B).

In sum, our work shows that loss of NOD2 significantly elevates E2 signaling levels in the intestine, that E2 exposure is sufficient to replicates all phenotypes associated with NOD2 deficiency, and that attenuation of E2 signaling restores epithelial homeostasis to NOD2-deficient fish, indicating estrogen signaling as a key modifier of the disruptions found in *nod2*$^{-/-}$ guts.

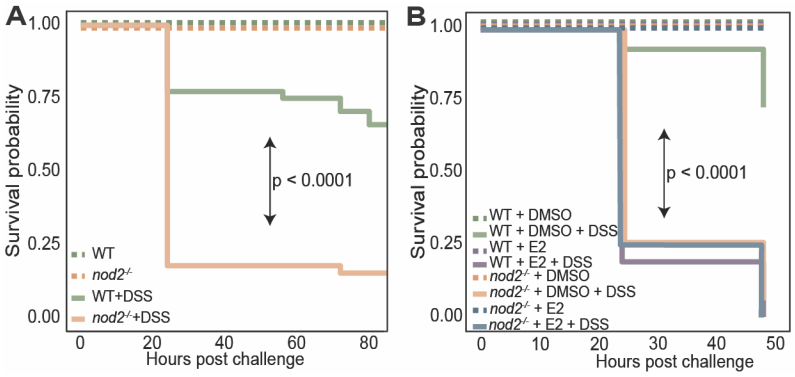

Fig 7. Estrogen modulates the survivability of DSS-treated larvae in a NOD2-dependent manner. A) Kaplan–Meier survival curves comparing WT and *nod2*$^{-/-}$ larvae exposed to 0.5% DSS, with n = 20 larvae per group. *nod2*$^{-/-}$ larvae exhibit significantly reduced survival following DSS-induced intestinal injury relative to WT siblings, indicating heightened sensitivity to epithelial damage in the absence of NOD2. **B)** Survival analysis of WT and *nod2*$^{-/-}$ larvae pretreated with either DMSO or 17β-estradiol (E2)

beginning at 3 dpf, followed by 0.5% DSS exposure at 5 dpf. P-values were determined using the log-rank (Mantel-Cox) test.

DISCUSSION

Loss-of-function *NOD2* alleles are the single greatest genetic signature of Crohn's disease [4-9]. However, we only have a partial appreciation of the consequences of NOD2 deficiency for intestinal epithelial cell dynamics. We consider this an important gap in our understanding of the factors that promote a chronic inflammatory illness that continues to grow in frequency.

We used zebrafish to determine how NOD2 deficiency impacts homeostatic maintenance of the intestinal barrier. Fish guts are remarkably like their mammalian counterparts in terms of developmental regulation and cell type composition [29-41], and NOD2-deficient fish replicate key features of CD-like inflammatory disease [42,43]. We found that, like mouse models, NOD2 deficiency alone does not lead to overt inflammatory disease in fish, and that *nod2* genetic status has minimal impacts on gut microbiota composition [21], emphasizing the utility of fish as a genetically accessible model of NOD2 deficiency. As anticipated, we observed signs of immune dysregulation in hematopoietic, epithelial, and stromal compartments of *nod2* mutants, including altered expression of inflammatory cytokines and autophagy pathway components that are widely linked to CD. However, we also found that NOD2 deficiency affected epithelial renewal and organization in an estrogen-sensitive manner. These findings add to our mechanistic understanding of NOD2 gut function and raise unanswered questions for future studies.

How does NOD2 regulate intestinal epithelial cell dynamics? Working with co-housed, wildtype and *nod2* mutant siblings derived from a heterozygous in-cross, we showed that NOD2 deficiency leads to intestinal shortening, increased sensitivity to DSS-induced damage, and reduced cell survival. Our results match findings from *NOD2* mutant mice and patient data, which show altered intestinal permeability [12,13], and increased susceptibility to inflammatory injury [24,25]. However, we do not yet know how loss of NOD2 translates to barrier defects. Our transcriptional data revealed widespread dysregulation of genes linked to cell growth and differentiation in the NOD2-deficient epithelium, and our quantitative work showed that NOD2 is necessary for epithelial proliferation and maturation. However, we also discovered shifts in the transcriptional landscape of genes required for cell survival, and we found that NOD2 deficiency resulted in significant death of mature epithelial cells. Therefore,

future studies using lineage tracing and cell-fate labeling strategies are required to resolve the extent to which cell proliferation, differentiation and survival accounts for barrier defects in *nod2* mutants.

How do NOD2 and estrogen interact at the epithelial barrier? One of the most striking findings from our transcriptomic analysis was a pronounced increase of estrogen signaling in *nod2*$^{-/-}$ intestines. Confirming links between NOD2 deficiency, estrogen signaling, and gut patterning, we showed that exposure to E2 attenuates epithelial proliferation and diminishes generation of goblet cells in wildtype larvae, whereas tamoxifen restores proliferation and goblet cell generation in NOD2-deficient larvae. Further supporting a mechanistic link between NOD2 and estrogen signaling, an earlier study showed that bazedoxifene reduces fibrosis, prevents epithelial hypertrophy, and suppresses pro-inflammatory cytokine expression in *nod2* mutants treated with DSS [43]. Although that work employed bazedoxifene as gp130 antagonist, we feel it is important to highlight that this drug is primarily known as a selective estrogen response modulator, widely prescribed for managing postmenopausal osteoporosis in women [74]. Commonly associated with development of female secondary sexual characteristics, estrogen has non-gonadal roles in male and female somatic tissue, including in IBD [75]. Epidemiological data showed that women have a greater incidence of Crohn's disease and experience more extraintestinal comorbidities than men [76-78]. Confirming a causal relationship between estrogen and Crohn's disease, oral contraceptive pill usage significantly increases disease risk for women [79,80]. In the gut, estrogen engages the nuclear estrogen receptors ERα and ERβ to control expression of target genes and interacts with the membrane-bound G protein-coupled estrogen receptor, GPER, to modify cellular functions at the post-transcriptional level [81]. Mechanistically, animal and tissue culture work indicate that estrogen primarily signals through ERβ to arrest proliferation and enhance cell death [58-60], matching phenotypes noted in the current study, and leading us to hypothesize that estrogen promotes an accumulation of barrier defects in *nod2* mutants.

While our data support a functional interaction between NOD2 and estrogen, the molecular link remains unresolved. It is plausible that NOD2 influences estrogen receptor stability, localization, or downstream transcriptional activity, either directly or through intermediates such as MAPK or PI3K signaling, both of which are modulated by NOD2 [82,83] and have known interactions with estrogen

pathways [84-86]. Alternatively, loss of NOD2 may lead to compensatory estrogen receptor activation in response to epithelial stress. Investigating these mechanistic connections will be an important area for future work.

What about sex? Our initial transcriptomic analyses were conducted on mixed-sex populations to capture a comprehensive overview of NOD2-dependent effects. However, the emergence of a sex-specific estrogen response highlights the need for more targeted comparisons. Future studies will explicitly separate males and females to resolve sex-specific transcriptional programs and functional outcomes, with key assays, such as epithelial proliferation, differentiation, and cell survival to determine how NOD2 interacts with estrogen.

We feel our findings have particular relevance to CD. The discovery that NOD2 interacts with estrogen offers a mechanistic insight into how its loss might impair epithelial barrier function. Estrogen has been implicated in the sex-dependent pathophysiology of CD with notable age-dependent differences in onset and severity. In pediatric cases, girls often present earlier and more severely than boys [87]. In adults, women have lower CD incidence during reproductive years, but risk rises post-menopause [88-94]. Additional clinical data shows that symptoms fluctuate with menstrual cycles [95-97], and that irregular menstruation often precedes diagnosis [98]. Our finding that *nod2*$^{-/-}$ female fish exhibit exaggerated estrogen responses may help explain how the hormonal environment interacts with genetic susceptibility to shape disease risk.

Future studies should investigate whether this regulatory axis operates in other mucosal tissues or during hormonal transitions such as puberty, pregnancy, or menopause. Additionally, given the increasing interest in estrogen modulators as therapeutic agents, our results suggest that NOD2 genotype may influence responses to hormone-based therapies and should be considered in precision medicine approaches to IBD.

ACKNOWLEDGMENTS

We acknowledge support with single-cell library preparation from Mike Wong at the Faculty of Medicine and Dentistry Advanced Cell Exploration (ACE) Core. We acknowledge flow cytometry support from Dr. Aja Rieger, Rikus Niemand, Lai Xu, and Xinyue Xu. Flow Cytometry Facility experiments were performed at the University of Alberta Faculty of Medicine & Dentistry Flow Cytometry Facility, which receives financial support from the Faculty of Medicine & Dentistry and Canada Foundation for Innovation (CFI) awards to contributing investigators. We acknowledge microscopy support from Dr. Hilmar Strickfaden, and Kiera Smith at the Faculty of Medicine and Dentistry Cell Imaging Core. We acknowledge the immunohistochemistry support provided by Dr. Kacie Norton at the Department of Biological Sciences Advanced Microscopy Facility. We would also like to thank Science Animal Support Services and the Alberta Health Sciences Animal Laboratory Services for their excellent care of the zebrafish aquatic facilities. We acknowledge Sanger DNA sequencing and HRM analysis support from Troy Locke at the Facility of Science Molecular Biology Facility (MBSU). Thanks to Dr. Dana Philpott, Derek Tsang, Dr. Lisa Willis, Lena Jones, Dr. Aurélia Joly, and Dr. Reegan Willms for critical reading of the manuscript. This work was supported by a grant from the Canadian Institutes of Health Research to E.F. M.E. has funding support through the Boytzun Studentship in Colorectal Cancer, Cancer Research Institute of Northern Alberta (CRINA), and Li Ka Shing Institute of Virology Graduate Studies Entrance Award.

AUTHOR CONTRIBUTIONS

M.E. and E.F. conceived and designed the experiments. M.E carried out the experiments. M.E. and E.F. performed computational analysis. Funding for this project was acquired by E.F. M.E. and E.F. wrote the manuscript.

DECLARATION OF INTERESTS

The authors declare no competing interests.

MATERIALS AND METHODS

Zebrafish strains and maintenance

All zebrafish experiments were performed at the University of Alberta using protocols approved by the University's Animal Care & Use Committees, Biosciences and Health Sciences (#3032), operating under the guidelines of the Canadian Council of Animal Care. Wild-type (TL) and *nod2*$^{-/-}$ knockout zebrafish (four to nine months-old; approx. equal sex distribution) were reared at 29°C in tank water (Instant Ocean Sea Salt dissolved in reverse osmosis water maintained at a conductivity of 1000µS and pH buffered to pH 7.0 with sodium bicarbonate) under a 14h/10h light/dark cycle using standard zebrafish husbandry protocols. Feeding regimens were age specific. From 6-14 days post-fertilization (dpf), larvae were fed GEMMA Micro 75 twice daily and live rotifers once daily. From 15-28 dpf, larvae received a 1:1 mixture of GEMMA Micro 75 and GEMMA Micro 150 twice daily, along with live rotifers once daily. Juvenile fish (29 dpf to 13 weeks) were fed GEMMA Micro 300 twice daily and live rotifers once daily. Adult zebrafish were maintained on a once-daily diet of GEMMA Micro 300 and live rotifers. For larval analysis, breeding tanks were set up overnight with 1 male and 1 female separated by a divider until morning. Fish were bred for 1 hour, then embryos were collected, rinsed gently with facility water, and transferred to a petri dish (fisherbrand) with 30 mL embryo media (EM) and 30 embryos per dish. Embryos were raised at 29°C under a 14 hour/ 10 hour light/ dark cycle until 7 dpf.

Generation and Validation of the *nod2*-mutant zebrafish line

crRNA:tracrRNA duplex and gRNA:Cas9 RNP complexes were prepared with the *nod2* crRNA sequence: TTGGACCTGCTACTTGCTC. Generation and validation of the *nod2*-mutant zebrafish line was performed as previously described [43], with modifications detailed below. Briefly, Wild-type TL zebrafish embryos were microinjected at the 1-4-cell stage with 1 nL of the CRISPR-Cas9 injection mix per embryo, using a reduced injection volume compared to the original protocol. At 5 days post-fertilization (dpf), larvae were collected for genomic DNA extraction. The genomic region encompassing the CRISPR target site was amplified by PCR, purified, and subjected to Sanger sequencing to assess mutation efficiency. Embryos with evidence of CRISPR-Cas9-induced mutations were raised to adulthood and outcrossed to wild-type TL zebrafish. Genomic DNA was extracted from F1 larvae at 5 dpf and screened for germline transmission of *nod2* mutations using high-resolution melting (HRM) analysis. Clutches positive for mutations were raised to adulthood, and heterozygous carriers were identified by HRM, PCR, and Sanger sequencing. Founder fish harboring the same mutation were selected and in-crossed, and F2 embryos were sequenced to confirm the presence of the intended mutation. The resultant mutant line carried a 4-base pair deletion (CTTG) in exon 2 of *nod2*, resulting in a frameshift and truncated, non-functional protein.

Generating single-cell suspensions for single cell RNA-sequencing

Single-cell suspensions were prepared from adult zebrafish intestines as previously described [31], with minor modifications. Briefly, five adult WT TL and five adult *nod2*$^{-/-}$ cohoused in-crossed siblings with equal sex distribution (2 males:3 females) were selected for tissue collection. Intestines were dissected, minced, and digested in a dissociation cocktail containing fresh collagenase A (1 mg/mL), 40µg/mL Proteinase K, and 10X Trypsin (0.25% final). Following digestion, cell suspensions were washed, filtered, and live cells isolated using OptiPrep Density Gradient Medium according to OptiPrep Application Sheet C13. Viable cells were counted and processed for single-cell RNA sequencing as described [31]. Cell suspensions were then diluted to a concentration of 1200 cell/µL and immediately run through the 10X Genomics Chromium Controller with Chromium Single Cell 3′ Library & Gel Bead Kit v3.1. Library QC and sequencing was performed by Novogene using the Illumina HiSeq platform.

Processing and analysis of single-cell RNA-seq data

Single-cell RNA-seq data were processed and analyzed as previously described [31], with minor modifications. Briefly, Cell Ranger v7.0.1 (10X Genomics) was used to demultiplex raw sequencing files and align reads to the zebrafish reference genome (Ensembl GRCz11.96). Cell Ranger output matrices

were analyzed using the Seurat R package (v5.0.1) [66] in RStudio. Cells with fewer than 200 unique molecular identifiers (UMIs), greater than 2500 UMIs, or greater than 25% mitochondrial reads were removed. Seurat was used to normalize expression values and perform clustering (resolution 0.8, 50 principal components), with optimal PCs determined by JackStraw scores [67] and elbow plots. Marker genes were identified using the "FindMarkers" function, and clusters were annotated using known zebrafish cell type markers or mammalian orthologs.

16S rRNA gene sequencing

Briefly, four adult WT TL and four *nod2*$^{-/-}$ cohoused in-crossed siblings with equal sex distribution were selected and fasted prior to dissections. Zebrafish intestines were dissected with surrounding organs removed. Individual guts were collected and homogenized in 300µL of Powerbead Solution. The Qiagen DNeasy UltraClean Microbial Kit (Cat No. 12224-250) was used to extract microbial DNA. To assess the intestinal bacterial community composition, the V4 variable region of the 16s rRNA gene encompassed by the 515 forward primer and 806 reverse primer was sequenced. Quality control and sequencing was performed by Novogene Corporation using illumina Novaseq Platform PE250. Sequences were processed with QIIME2-2024.10 [68]. The DADA2 pipeline was used to join paired-end reads, remove chimeric sequences, and to generate the feature table used to resolve amplicon sequence variants using default parameters. DADA2 denoising resulted in 770,832 reads. Amplicon sequence variants (ASVs) represented by fewer than 200 reads across all samples were removed. A naïve Bayes classifier trained on SILVA138 99% full-length reference sequences was used to assign taxonomy. Taxonomy assignments were verified using NCBI blast. The sequence table was then filtered to exclude any sequences that were unassigned, not assigned past phylum level, or assigned as eukaryota, resulting in 673,162 sequences corresponding to 78 unique features.

RNA extraction and cDNA Synthesis

Total RNA was extracted from zebrafish intestinal tissue using TRIzol Reagent (Thermo Fisher Scientific) following manufacturer protocols with minor modifications. Intestinal samples were collected from five WT TL males, five WT TL females, five *nod2*$^{-/-}$ males, and five *nod2*$^{-/-}$ females, all derived from cohoused in-crossed sibling groups. Fish were fasted prior to dissection. Individual intestines were isolated, cleared of surrounding tissue, and homogenized in 250 µL of TRIzol using a motorized pestle. Homogenates were brought to 1 mL total volume with additional TRIzol and stored at -70 °C until further processing. For phase separation, 400 µL of chloroform was added, followed by 15 s vortexing and a 3-minute incubation at room temperature. The aqueous phase was collected, and chloroform extraction was repeated at a 1:1 ratio. RNA was precipitated by adding 50 µL of 3 M sodium acetate (pH 5.2) and 1 mL of 95% ethanol, followed by overnight incubation at 4 °C. RNA was pelleted by centrifugation (12,000 × g, 10 min, 4 °C), washed twice in 0.5 mL 75% ethanol (7,500 × g, 10 min, 4 °C), and resuspended in 50 µL of nuclease-free water. RNA concentrations were determined using a NanoDrop spectrophotometer and diluted to a standardized concentration for downstream cDNA synthesis. cDNA was synthesized from up to 3 µg of total RNA using the qScript cDNA SuperMix (Quantabio, no. 95048-100) in a total reaction volume of 20 µL. Reactions were incubated at 25 °C for 5 min, 42 °C for 30 min, and 85 °C for 5 min, followed by a 4 °C hold.

Quantitative RT-qPCR

Quantitative PCR was performed using PerfeCTa SYBR Green SuperMix (Quantabio, no. 95054-500) on a One-Step real-time PCR thermocycler. Reactions were carried out in a 10 µL volume containing 2.5 µL of cDNA and 1.6 µM of each forward and reverse primer. Plates were centrifuged at 200 × g for 1 minute prior to thermocycling. The qPCR program consisted of an initial denaturation at 95 °C for 3 minutes, followed by 40 amplification cycles of 95 °C for 15 seconds and 60 °C for 45 seconds, with melt curve analysis included at the end of the run. All reactions were performed in

technical triplicates. Cycle threshold (Ct) values were averaged across replicates, and relative gene expression was calculated using the ΔΔCt method, with *ef1α* used as the endogenous reference gene.

Zebrafish RT-qPCR primer sequences

The following sequences were used (given in order from the 5′ to 3′ end): *vtg1* qPCR forward, GCCAAAAAGCTGGGTAAACA; *vtg1* qPCR reverse, AGTTCCGTCTGGATTGATGG; *vtg2* qPCR forward, TGCCGCATGAAACTTGAATCT; *vtg2* qPCR reverse, GTTCTTACTGGTGCACAGCC; *vtg4* qPCR forward, TCCAGACGGTACTTTCACCA; *vtg4* qPCR reverse, CTGACAGTTCTGCATCAACACA; *ef1a* qPCR forward, GCATACACTAAGAAGATCGGC; *ef1a* qPCR reverse, TCTTCCATCCCTTGAACCAG. *vtg* qPCR primer sequences were obtained from Muncke et al (2006) [69] and Yilmaz et al (2019) [70]

Generating germ-free zebrafish

Fish embryos were made germ-free as described in [39]. A clutch of embryos was collected then washed and split into two cohorts. The CV cohort was kept in sterile EM, while the GF cohort was kept in sterile EM supplemented with ampicillin (100 µg/mL), kanamycin (5 µg/mL), amphotericin B (250 ng/mL), and gentamicin (50 µg/mL). Embryos were washed every 2 hours with EM or EM plus antibiotics for CV and GF cohorts respectively. Once at 50% epiboly, the GF cohort was successively washed three times in EM, then 2 minutes in 0.1% polyvinylpyrrolidone-iodine (PVP-I) in EM, followed by three EM washes, then a 20-minute incubation with 0.003% sodium hypochlorite (bleach) in EM. Embryos were washed three more times then transferred into tissue culture flasks with sterile EM. The CV cohort received the same number and duration of washes, using EM in lieu of dilute PVP-I or bleach. All work was performed in a biosafety cabinet sterilized first with 10% bleach, followed by 70% ethanol. We tested for bacterial contamination in GF flasks at 4 days post-fertilization, according to established protocol. EM was collected from CV and GF culture flasks to test for bacteria by plating on TSA. Parental tank water and sterile filtered water were used as a positive and negative control respectively, where bacteria were positively identified in parental tank water and confirmed absent from sterile water. CV and GF flasks with bacteria present or absent respectively were used for subsequent analysis.

Flow Cytometry of Intestinal Proliferation in Zebrafish Larvae

To quantify intestinal epithelial proliferation, zebrafish larvae were immersed in 100 µg/mL 5-ethynyl-2'-deoxyuridine (EdU; 10 mM stock in DMSO) for 24 hours in embryo medium containing 1% DMSO, with or without muramyl dipeptide (MDP) at 1 µg/mL. A 10 mg/ml working stock of MDP (Sigma-Aldrich A9519) was diluted to 1 µg/ml for all treatments. For MDP treatments, axenic larvae were exposed to MDP for 16 hrs prior to EdU labeling. Following treatment, intestines were dissected from 15 larvae per condition in ice-cold PBS and subjected to enzymatic dissociation in a cocktail containing 1 mg/mL collagenase, 0.25% trypsin, and 40 µg/mL proteinase K at 37°C for 30 minutes with intermittent gentle trituration. Dissociated cells were filtered through a 40 µm strainer, pelleted by centrifugation (300 × g, 10 min, 4°C), and washed with PBS. Cells were fixed in 4% paraformaldehyde for 15 minutes at room temperature, washed with FACS buffer (PBS without calcium or magnesium supplemented with 2% heat-inactivated calf serum), and permeabilized in saponin buffer (0.1% saponin in FACS buffer) for 10 minutes. EdU detection was performed using the Click-iT® EdU Alexa Fluor 488 Imaging Kit according to the manufacturer's instructions. After EdU labeling, cells were stained with DRAQ5 (1:1000) for nuclear visualization. Flow cytometry was conducted on the Attune NxT cytometer, and EdU^+ proliferating cells were quantified based on fluorescence intensity using appropriate controls for gating.

Estrogen and Tamoxifen treatment of zebrafish larvae

A working stock of 20mg/mL 17β-estradiol (E2; Sigma) was prepared in DMSO and diluted to a final concentration of 25 ng/μL in 1xEM for all treatments. No more than 20 zebrafish larvae at 5 dpf were placed in each petri dish and incubated in 25 ng/μL E2 or control DMSO for 24 hrs. Larvae were then collected for downstream applications, including immunofluorescence and whole- mount Alcian blue staining. Similarly, a 20mg/mL stock of tamoxifen (Sigma), dissolved in DMSO, was diluted to a final concentration of 1.5 ng/μL in 1xEM. Larvae (5 dpf; ≤20 per dish) were incubated in 1.5 ng/μL tamoxifen for 6 hrs prior to collection for EdU labeling and Alcian blue staining. For DSS survival assays, larvae were pretreated with E2 for 24 hrs or tamoxifen for 6 hrs before initiating DSS exposure.

DSS treatment of zebrafish larvae

DSS treatments were performed as previously described [71], with 0.5% DSS (Sigma, cat. no. 42867) used for all experiments and treatments initiated at 5 dpf. Briefly, no more than 20 zebrafish larvae were placed in each petri dish and incubated in freshly prepared 0.5% DSS dissolved in 1x EM for 24 hrs. Larvae were collected for further experimental use after removal of DSS. For survival assays, larvae were continuously exposed to 0.5% DSS in 1x EM beginning at 5 dpf. Media was replaced daily by transferring larvae into fresh DSS-containing petri dishes. Survival was monitored over time and quantified by Kaplan-Meier analysis, using 20 larvae per genotype per condition

Whole-mount alcian blue staining of zebrafish larvae

This protocol was adapted and modified from [71]. To visualize goblet cells, whole zebrafish larvae were fixed in 4% paraformaldehyde (PFA) at 4°C for 48 hours. Fixed larvae were transferred into a 70 μm nylon mesh cell strainer and rinsed in 1× PBS for 5 minutes, followed by a 10-minute incubation in acidic ethanol (70% ethanol containing 1% concentrated HCl). Larvae were stained with 0.1% Alcian blue solution (prepared in 3% acetic acid, pH 2.5) for 3 hours at room temperature, then washed three times with acidic ethanol, followed by an overnight incubation. Larvae were mounted in 0.7% low-melting-point agarose and imaged. Alcian blue-positive intestinal regions were quantified in Fiji (ImageJ) using blinded analysis. Images were converted to RGB and thresholded to isolate Alcian blue-positive regions within the mid- and distal gut, and area measurements were obtained using particle analysis tools.

Immunofluorescence and fluorescence microscopy

Adult zebrafish intestines were fixed in 4% PFA (diluted in 1xPBS) overnight at 4°C. Intestines were washed twice in 1xPBS. Intestinal segments were then cryoprotected in 15% (w/v) sucrose/PBS at room temperature until sunk followed by sinking in 30% (w/v) sucrose/PBS (overnight at 4°C). Intestines were mounted in Optimal Cutting Temperature Embedding Medium, then frozen on dry ice. Seven-micron cryosections were collected on Superfrost Plus slides. After allowing sections to adhere onto slides, slides were immersed in PBS for 20 min at room temperature. Tissue was blocked for 1hr at room temperature in 3% (w/v) BSA dissolved in PBST (1xPBS +0.2% (v/v) Tween 20). Primary antibodies were diluted in blocking buffer. Sections were incubated in primary antibody solution overnight in a humid chamber at 4°C. The primary antibody used in this paper was mouse anti-zebrafish gut secretory cell epitopes antibody [FIS 2F11/2] 1/500 (abcam 71286). Excess primary antibody was washed by immersing slides in fresh PBST for 1.5hrs. Sections were incubated in secondary antibody solution (prepared in blocking buffer) for 1hr at room temperature in a humid chamber, protected from light. To stain apoptotic cells, secondary solution was removed then sections incubated in TUNEL reaction mixture following the manufacturer's suggestion (Roche 12156792910). Lastly, nuclei were stained with Hoechst (Molecular Probes Cat# H-3569) diluted 1:2000 in PBST for 10 min protected from light. Slides were washed in PBST by brief immersion followed by a 30-min incubation in fresh PBST protected from light. Slides were mounted in Fluoromount Aqueous Mounting Medium.

Zebrafish larvae (6-7 dpf) were incubated in embryo medium with 1% DMSO and 5 mM EdU for 8 hrs at 29°C. Fish intestines were dissected in PBS and fixed in 4% paraformaldehyde in PBS overnight

at 4°C. Guts were washed three times with PBSTx (0.75% Triton X-100 in 1X PBS), blocked for 1 hr in PBSTx +3% BSA at room temperature, and stained with primary antibodies in blocking buffer overnight at 4°C. Guts were washed with PBSTx and then stained for 1 hr at room temperature with secondary antibodies and nuclear stain (1/1000 Hoechst 33258), followed by rinse in PBSTx. EdU detection was performed by incubating guts in Click-iT reaction cocktail for 30 min at room temperature. Guts were washed in PBSTx followed by extra washing in PBS. Whole larval intestines were mounted on microscope slides using Flouromount and visualized

Immunohistochemistry

Adult zebrafish intestines were fixed at 4°C in BT fixative: 4% PFA, 0.15mM CaCl2, 4% Sucrose in 0.1 M phosphate buffer (pH 7.4). Intestinal segments were processed for paraffin embedding and 5µm sections collected on Superfrost Plus slides. Tissue was deparaffinized, rehydrated, then boiled in 10mM sodium citrate pH 6, 0.05% Tween 20 for 20 min at 98°C to unmask antigen. After cooling sections to room temperature for 30 min, sections were incubated in 3% hydrogen peroxide for 10 min, washed twice in dH2O, and once in PBSt (PBS +0.5% Triton X-100). Sections were then blocked for 1hr at room temperature in 10% (v/v) normal goat serum (NGS)/PBSt followed by overnight incubation in primary antibody solution (prepared in blocking buffer) in a humid chamber at 4°C. The primary antibodies used in this paper were: mouse anti-PCNA 1:5000 (Sigma P8825) and rabbit anti-Lcp1 1:1000 (GeneTex GTX124420). Slides were washed three times in PBSt and tissue incubated in SignalStain Boost Detection Reagent (HRP, Rabbit or Mouse) for 30 min at room temperature. Colorimetric detection was done by incubating in SignalStain DAB Chromogen solution for 5 min. Sections were counterstained with Alcian blue (Aldrich 19,978-8) for 3 mins, counterstained in quarter-strength Hematoxylin Gill III (Leica Ca.# 3801542) for 30 s, dehydrated in ethanol, cleared with toluene and mounted in DPX.

Microscopy

Histological samples were imaged on a ZEISS AXIO A1 compound light microscope with a SeBaCam 5.1MP camera. Confocal images were captured on an Olympus IX-81 microscope fitted with a CSU-X1 spinning disk confocal scan-head, Hamamatsu EMCCD (C9100-13) camera and operated with PerkinElmer's Volocity. Confocal z stack image processing was done in Fiji [72].

Quantification and statistical analysis

Statistical analyses were performed using R. The statistical tests, group statistics, and P values used in each experiment are described in the respective figure legends.

CITATIONS

1. Ng SC, Shi HY, Hamidi N, Underwood FE, Tang W, Benchimol EI, Panaccione R, Ghosh S, Wu JC, Chan FK, Sung JJ. Worldwide incidence and prevalence of inflammatory bowel disease in the 21st century: a systematic review of population-based studies. The Lancet. 2017 Dec 23;390(10114):2769-78.
2. Molodecky NA, Soon S, Rabi DM, Ghali WA, Ferris M, Chernoff G, Benchimol EI, Panaccione R, Ghosh S, Barkema HW, Kaplan GG. Increasing incidence and prevalence of the inflammatory bowel diseases with time, based on systematic review. Gastroenterology. 2012 Jan 1;142(1):46-54.
3. Solitano V, Bernstein CN, Dotan I, Dignass A, Domilici R, Dubinsky MC, Gearry RB, Hart A, Kaplan GG, Ma C, Magro F. Shaping the future of inflammatory bowel disease: a global research agenda for better management and public health response. Nature Reviews Gastroenterology & Hepatology. 2025 Apr 22:1-5.
4. Hugot JP, Chamaillard M, Zouali H, Lesage S, Cézard JP, Belaiche J, Almer S, Tysk C, O'Morain CA, Gassull M, Binder V. Association of NOD2 leucine-rich repeat variants with susceptibility to Crohn's disease. Nature. 2001 May 31;411(6837):599-603.
5. Ogura Y, Bonen DK, Inohara N, Nicolae DL, Chen FF, Ramos R, Britton H, Moran T, Karaliuskas R, Duerr RH, Achkar JP. A frameshift mutation in NOD2 associated with susceptibility to Crohn's disease. Nature. 2001 May 31;411(6837):603-6.
6. Jostins L, Ripke S, Weersma RK, Duerr RH, McGovern DP, Hui KY, Lee JC, Philip Schumm L, Sharma Y, Anderson CA, Essers J. Host–microbe interactions have shaped the genetic architecture of inflammatory bowel disease. Nature. 2012 Nov 1;491(7422):119-24.
7. Hugot JP, Laurent-Puig P, Gower-Rousseau C, Olson JM, Lee JC, Beaugerie L, Naom I, Dupas JL, Van Gossum A, Groupe d'Etude Therapeutique des Affections Inflammatoires Digestives, Orholm M. Mapping of a susceptibility locus for Crohn's disease on chromosome 16. Nature. 1996 Feb 29;379(6568):821-3.
8. Lesage S, Zouali H, Cézard JP, Colombel JF, Belaiche J, Almer S, Tysk C, O'Morain C, Gassull M, Binder V, Finkel Y. CARD15/NOD2 mutational analysis and genotype-phenotype correlation in 612 patients with inflammatory bowel disease. The American Journal of Human Genetics. 2002 Apr 1;70(4):845-57.
9. Horowitz JE, Warner N, Staples J, Crowley E, Gosalia N, Murchie R, Van Hout C, Fiedler K, Welch G, King AK, Reid JG. Mutation spectrum of NOD2 reveals recessive inheritance as a main driver of Early Onset Crohn’s Disease. Scientific reports. 2021 Mar 10;11(1):5595.
10. Choi PM, Zelig M. Similarity of colorectal cancer in Crohn's disease and ulcerative colitis: implications for carcinogenesis and prevention. Gut. 1994 Jul 1;35(7):950-
11. Branquinho D, Freire P, Sofia C. NOD2 mutations and colorectal cancer-Where do we stand?. World journal of gastrointestinal surgery. 2016 Apr 27;8(4):284.
12. Strober W, Watanabe T. NOD2, an intracellular innate immune sensor involved in host defense and Crohn's disease. Mucosal immunology. 2011 Sep;4(5):484-95.
13. Kobayashi KS, Chamaillard M, Ogura Y, Henegariu O, Inohara N, Nuñez G, Flavell RA. Nod2-dependent regulation of innate and adaptive immunity in the intestinal tract. Science. 2005 Feb 4;307(5710):731-4.
14. Wehkamp J, Harder J, Weichenthal M, Schwab M, Schäffeler E, Schlee M, Herrlinger KR, Stallmach A, Noack F, Fritz P, Schröder JM. NOD2 (CARD15) mutations in Crohn’s disease are associated with diminished mucosal α-defensin expression. Gut. 2004 Nov 1;53(11):1658-64.

15. Lala S, Ogura Y, Osborne C, Hor SY, Bromfield A, Davies S, Ogunbiyi O, Nuñez G, Keshav S. Crohn's disease and the NOD2 gene: a role for paneth cells. Gastroenterology. 2003 Jul 1;125(1):47-57.
16. Wehkamp J, Salzman NH, Porter E, Nuding S, Weichenthal M, Petras RE, Shen B, Schaeffeler E, Schwab M, Linzmeier R, Feathers RW. Reduced Paneth cell α-defensins in ileal Crohn's disease. Proceedings of the National Academy of Sciences. 2005 Dec 13;102(50):18129-34.
17. Perminow G, Beisner J, Koslowski M, Lyckander LG, Stange E, Vatn MH, Wehkamp J. Defective Paneth Cell—Mediated Host Defense in Pediatric Ileal Crohn's Disease. Official journal of the American College of Gastroenterology| ACG. 2010 Feb 1;105(2):452-9.
18. Girardin SE, Boneca IG, Viala J, Chamaillard M, Labigne A, Thomas G, Philpott DJ, Sansonetti PJ. Nod2 is a general sensor of peptidoglycan through muramyl dipeptide (MDP) detection. Journal of Biological Chemistry. 2003 Mar 14;278(11):8869-72.
19. Inohara N, Ogura Y, Fontalba A, Gutierrez O, Pons F, Crespo J, Fukase K, Inamura S, Kusumoto S, Hashimoto M, Foster SJ. Host recognition of bacterial muramyl dipeptide mediated through NOD2: implications for Crohn′ s disease. Journal of Biological Chemistry. 2003 Feb 21;278(8):5509-12.
20. Shanahan MT, Carroll IM, Grossniklaus E, White A, von Furstenberg RJ, Barner R, Fodor AA, Henning SJ, Sartor RB, Gulati AS. Mouse Paneth cell antimicrobial function is independent of Nod2. Gut. 2014 Jun 1;63(6):903-10.
21. Robertson SJ, Zhou JY, Geddes K, Rubino SJ, Cho JH, Girardin SE, Philpott DJ. Nod1 and Nod2 signaling does not alter the composition of intestinal bacterial communities at homeostasis. Gut microbes. 2013 May 1;4(3):222-31.
22. Simms LA, Doecke JD, Walsh MD, Huang N, Fowler EV, Radford-Smith GL. Reduced α-defensin expression is associated with inflammation and not NOD2 mutation status in ileal Crohn's disease. Gut. 2008 Jul 1;57(7):903-10.
23. Cruickshank SM, Wakenshaw L, Cardone J, Howdle PD, Murray PJ, Carding SR. Evidence for the involvement of NOD2 in regulating colonic epithelial cell growth and survival. World Journal of Gastroenterology: WJG. 2008 Oct 14;14(38):5834.
24. Nigro G, Rossi R, Commere PH, Jay P, Sansonetti PJ. The cytosolic bacterial peptidoglycan sensor Nod2 affords stem cell protection and links microbes to gut epithelial regeneration. Cell host & microbe. 2014 Jun 11;15(6):792-8.
25. Zanello G, Goethel A, Rouquier S, Prescott D, Robertson SJ, Maisonneuve C, Streutker C, Philpott DJ, Croitoru K. The cytosolic microbial receptor Nod2 regulates small intestinal crypt damage and epithelial regeneration following T cell–induced enteropathy. The Journal of Immunology. 2016 Jul 1;197(1):345-55.
26. Schwarzer M, Gautam UK, Makki K, Lambert A, Brabec T, Joly A, Šrůtková D, Poinsot P, Novotná T, Geoffroy S, Courtin P. Microbe-mediated intestinal NOD2 stimulation improves linear growth of undernourished infant mice. Science. 2023 Feb 24;379(6634):826-33.
27. Brugman S. The zebrafish as a model to study intestinal inflammation. Developmental & Comparative Immunology. 2016 Nov 1;64:82-92.
28. Flores EM, Nguyen AT, Odem MA, Eisenhoffer GT, Krachler AM. The zebrafish as a model for gastrointestinal tract–microbe interactions. Cellular microbiology. 2020 Mar;22(3):e13152.
29. Willms RJ, Foley E. Mechanisms of epithelial growth and development in the zebrafish intestine. Biochemical Society Transactions. 2023 Jun 28;51(3):1213-24.
30. Willms RJ, Jones LO, Hocking JC, Foley E. A cell atlas of microbe-responsive processes in the zebrafish intestine. Cell Reports. 2022 Feb 1;38(5).

31. Jones LO, Willms RJ, Xu X, Graham RD, Eklund M, Shin M, Foley E. Single-cell resolution of the adult zebrafish intestine under conventional conditions and in response to an acute Vibrio cholerae infection. Cell reports. 2023 Nov 28;42(11).
32. Crosnier C, Vargesson N, Gschmeissner S, Ariza-McNaughton L, Morrison A, Lewis J. Delta-Notch signalling controls commitment to a secretory fate in the zebrafish intestine.
33. Grunwald DJ, Eisen JS. Headwaters of the zebrafish—emergence of a new model vertebrate. Nature reviews genetics. 2002 Sep 1;3(9):717-24.
34. Wallace KN, Pack M. Unique and conserved aspects of gut development in zebrafish. Developmental biology. 2003 Mar 1;255(1):12-29.
35. Wallace KN, Akhter S, Smith EM, Lorent K, Pack M. Intestinal growth and differentiation in zebrafish. Mechanisms of development. 2005 Feb 1;122(2):157-73.
36. Rawls JF, Samuel BS, Gordon JI. Gnotobiotic zebrafish reveal evolutionarily conserved responses to the gut microbiota. Proceedings of the National Academy of Sciences. 2004 Mar 30;101(13):4596-601.
37. Lickwar CR, Camp JG, Weiser M, Cocchiaro JL, Kingsley DM, Furey TS, Sheikh SZ, Rawls JF. Genomic dissection of conserved transcriptional regulation in intestinal epithelial cells. PLoS biology. 2017 Aug 29;15(8):e2002054.
38. Kanther M, Sun X, Mühlbauer M, Mackey LC, Flynn III EJ, Bagnat M, Jobin C, Rawls JF. Microbial colonization induces dynamic temporal and spatial patterns of NF-κB activation in the zebrafish digestive tract. Gastroenterology. 2011 Jul 1;141(1):197-207.
39. Melancon E, Canny SG, Sichel S, Kelly M, Wiles TJ, Rawls JF, Eisen JS, Guillemin K. Best practices for germ-free derivation and gnotobiotic zebrafish husbandry. Methods in cell biology. 2017 Jan 1;138:61-100.
40. Bates JM, Mittge E, Kuhlman J, Baden KN, Cheesman SE, Guillemin K. Distinct signals from the microbiota promote different aspects of zebrafish gut differentiation. Developmental biology. 2006 Sep 15;297(2):374-86.
41. Cheesman SE, Neal JT, Mittge E, Seredick BM, Guillemin K. Epithelial cell proliferation in the developing zebrafish intestine is regulated by the Wnt pathway and microbial signaling via Myd88. Proceedings of the National Academy of Sciences. 2011 Mar 15;108(supplement_1):4570-7.
42. Oehlers SH, Flores MV, Hall CJ, Swift S, Crosier KE, Crosier PS. The inflammatory bowel disease (IBD) susceptibility genes NOD1 and NOD2 have conserved anti-bacterial roles in zebrafish. Disease models & mechanisms. 2011 Nov 1;4(6):832-41.
43. Nayar S, Morrison JK, Giri M, Gettler K, Chuang LS, Walker LA, Ko HM, Kenigsberg E, Kugathasan S, Merad M, Chu J. A myeloid–stromal niche and gp130 rescue in NOD2-driven Crohn's disease. Nature. 2021 May 13;593(7858):275-81.
44. Uribe-Salazar JM, Kaya G, Sekar A, Weyenberg K, Ingamells C, Dennis MY. Evaluation of CRISPR gene-editing tools in zebrafish. BMC genomics. 2022 Dec;23:1-6.
45. Hoshijima K, Jurynec MJ, Shaw DK, Jacobi AM, Behlke MA, Grunwald DJ. Highly efficient CRISPR-Cas9-based methods for generating deletion mutations and F0 embryos that lack gene function in zebrafish. Developmental cell. 2019 Dec 2;51(5):645-57.
46. Haber AL, Biton M, Rogel N, Herbst RH, Shekhar K, Smillie C, Burgin G, Delorey TM, Howitt MR, Katz Y, Tirosh I. A single-cell survey of the small intestinal epithelium. Nature. 2017 Nov 16;551(7680):333-9.
47. Neurath MF. Cytokines in inflammatory bowel disease. Nature Reviews Immunology. 2014 May;14(5):329-42.

48. Guan Q. A comprehensive review and update on the pathogenesis of inflammatory bowel disease. Journal of immunology research. 2019;2019(1):7247238.
49. Shaw MH, Reimer T, Sánchez-Valdepeñas C, Warner N, Kim YG, Fresno M, Nuñez G. T cell–intrinsic role of Nod2 in promoting type 1 immunity to Toxoplasma gondii. Nature immunology. 2009 Dec;10(12):1267-74.
50. Petterson T, Jendholm J, Månsson A, Bjartell A, Riesbeck K, Cardell LO. Effects of NOD-like receptors in human B lymphocytes and crosstalk between NOD1/NOD2 and Toll-like receptors. Journal of leukocyte biology. 2011 Feb;89(2):177-87.
51. Hedl M, Li J, Cho JH, Abraham C. Chronic stimulation of Nod2 mediates tolerance to bacterial products. Proceedings of the National Academy of Sciences. 2007 Dec 4;104(49):19440-5.
52. Cooney R, Baker J, Brain O, Danis B, Pichulik T, Allan P, Ferguson DJ, Campbell BJ, Jewell D, Simmons A. NOD2 stimulation induces autophagy in dendritic cells influencing bacterial handling and antigen presentation. Nature medicine. 2010 Jan;16(1):90-7.
53. Brain O, Owens BM, Pichulik T, Allan P, Khatamzas E, Leslie A, Steevels T, Sharma S, Mayer A, Catuneanu AM, Morton V. The intracellular sensor NOD2 induces microRNA-29 expression in human dendritic cells to limit IL-23 release. Immunity. 2013 Sep 19;39(3):521-36.
54. Ramanan D, San Tang M, Bowcutt R, Loke PN, Cadwell K. Bacterial sensor Nod2 prevents inflammation of the small intestine by restricting the expansion of the commensal Bacteroides vulgatus. Immunity. 2014 Aug 21;41(2):311-24.
55. Vyhlidal CA, Chapron BD, Ahmed A, Singh V, Casini R, Shakhnovich V. Effect of Crohn's disease on villous length and CYP3A4 expression in the pediatric small intestine. Clinical and translational science. 2021 Mar;14(2):729-36.
56. Gersemann M, Becker S, Kübler I, Koslowski M, Wang G, Herrlinger KR, Griger J, Fritz P, Fellermann K, Schwab M, Wehkamp J. Differences in goblet cell differentiation between Crohn's disease and ulcerative colitis. Differentiation. 2009 Jan 1;77(1):84-94.
57. Menuet A, Pellegrini E, Anglade I, Blaise O, Laudet V, Kah O, Pakdel F. Molecular characterization of three estrogen receptor forms in zebrafish: binding characteristics, transactivation properties, and tissue distributions. Biology of reproduction. 2002 Jun 1;66(6):1881-92.
58. Looijer-van Langen M, Hotte N, Dieleman LA, Albert E, Mulder C, Madsen KL. Estrogen receptor-β signaling modulates epithelial barrier function. American Journal of Physiology-Gastrointestinal and Liver Physiology. 2011 Apr;300(4):G621-6.
59. Pettersson K, Delaunay F, Gustafsson JÅ. Estrogen receptor β acts as a dominant regulator of estrogen signaling. Oncogene. 2000 Oct;19(43):4970-8.
60. Wada-Hiraike O, Imamov O, Hiraike H, Hultenby K, Schwend T, Omoto Y, Warner M, Gustafsson JÅ. Role of estrogen receptor β in colonic epithelium. Proceedings of the National Academy of Sciences. 2006 Feb 21;103(8):2959-64.
61. Wesselman HM, Wingert RA. Estrogen signaling in development: recent insights from the zebrafish. The International Journal of Developmental Biology. 2024 Feb 22;68(1):1-7.
62. Green JM, Lange A, Scott A, Trznadel M, Wai HA, Takesono A, Brown AR, Owen SF, Kudoh T, Tyler CR. Early life exposure to ethinylestradiol enhances subsequent responses to environmental estrogens measured in a novel transgenic zebrafish. Scientific Reports. 2018 Feb 9;8(1):2699.
63. Takahashi H. Juvenile hermaphroditism in the zebrafish, Brachydanio rerio. Bulletin of the Faculty of Fisheries Hokkaido University. 1977;28.
64. Hsiao CD, Tsai HJ. Transgenic zebrafish with fluorescent germ cell: a useful tool to visualize germ cell proliferation and juvenile hermaphroditism in vivo. Developmental biology. 2003 Oct 15;262(2):313-23.

65. Xia L, Zheng L, Zhou JL. Transcriptional and morphological effects of tamoxifen on the early development of zebrafish (Danio rerio). Journal of Applied Toxicology. 2016 Jun;36(6):853-62.
66. Hao Y, Hao S, Andersen-Nissen E, Mauck WM, Zheng S, Butler A, Lee MJ, Wilk AJ, Darby C, Zager M, Hoffman P. Integrated analysis of multimodal single-cell data. Cell. 2021 Jun 24;184(13):3573-87.
67. Macosko EZ, Basu A, Satija R, Nemesh J, Shekhar K, Goldman M, Tirosh I, Bialas AR, Kamitaki N, Martersteck EM, Trombetta JJ. Highly parallel genome-wide expression profiling of individual cells using nanoliter droplets. Cell. 2015 May 21;161(5):1202-14.
68. Bolyen E, Rideout JR, Dillon MR, Bokulich NA, Abnet CC, Al-Ghalith GA, Alexander H, Alm EJ, Arumugam M, Asnicar F, Bai Y. Reproducible, interactive, scalable and extensible microbiome data science using QIIME 2. Nature biotechnology. 2019 Aug;37(8):852-7.
69. Muncke J, Eggen RI. Vitellogenin 1 mRNA as an early molecular biomarker for endocrine disruption in developing zebrafish (Danio rerio). Environmental Toxicology and Chemistry. 2006 Oct 1;25(10):2734-41.
70. Yilmaz O, Patinote A, Nguyen T, Com E, Pineau C, Bobe J. Genome editing reveals reproductive and developmental dependencies on specific types of vitellogenin in zebrafish (Danio rerio). Molecular reproduction and development. 2019 Sep;86(9):1168-88.
71. Oehlers SH, Flores MV, Hall CJ, Okuda KS, Sison JO, Crosier KE, Crosier PS. Chemically induced intestinal damage models in zebrafish larvae. Zebrafish. 2013 Jun 1;10(2):184-93.
72. Schindelin J, Arganda-Carreras I, Frise E, Kaynig V, Longair M, Pietzsch T, Preibisch S, Rueden C, Saalfeld S, Schmid B, Tinevez JY. Fiji: an open-source platform for biological-image analysis. Nature methods. 2012 Jul;9(7):676-82.
73. Amendola A, Butera A, Sanchez M, Strober W, Boirivant M. Nod2 deficiency is associated with an increased mucosal immunoregulatory response to commensal microorganisms. Mucosal immunology. 2014 Mar 1;7(2):391-404.
74. Raina, P. M., Patel, P. & Parmar, M. Bazedoxifene. in StatPearls (StatPearls Publishing, Treasure Island (FL), 2024).
75. Goodman WA, Erkkila IP, Pizarro TT. Sex matters: impact on pathogenesis, presentation and treatment of inflammatory bowel disease. Nature reviews Gastroenterology & hepatology. 2020 Dec;17(12):740-54.
76. Bernstein CN, Wajda A, Svenson LW, MacKenzie A, Koehoorn M, Jackson M, Fedorak R, Israel D, Blanchard JF. The epidemiology of inflammatory bowel disease in Canada: a population-based study. Official journal of the American College of Gastroenterology| ACG. 2006 Jul 1;101(7):1559-68.
77. Lophaven SN, Lynge E, Burisch J. The incidence of inflammatory bowel disease in Denmark 1980–2013: a nationwide cohort study. Alimentary pharmacology & therapeutics. 2017 Apr;45(7):961-72.
78. Betteridge JD, Armbruster SP, Maydonovitch C, Veerappan GR. Inflammatory bowel disease prevalence by age, gender, race, and geographic location in the US military health care population. Inflammatory bowel diseases. 2013 Jun 1;19(7):1421-7.
79. Ortizo R, Lee SY, Nguyen ET, Jamal MM, Bechtold MM, Nguyen DL. Exposure to oral contraceptives increases the risk for development of inflammatory bowel disease: a meta-analysis of case-controlled and cohort studies. European journal of gastroenterology & hepatology. 2017 Sep 1;29(9):1064-70.

80. Cornish JA, Tan E, Simillis C, Clark SK, Teare J, Tekkis PP. The risk of oral contraceptives in the etiology of inflammatory bowel disease: a meta-analysis. Official journal of the American College of Gastroenterology| ACG. 2008 Sep 1;103(9):2394-400.
81. Chen C, Gong X, Yang X, Shang X, Du Q, Liao Q, Xie R, Chen Y, Xu J. The roles of estrogen and estrogen receptors in gastrointestinal disease. Oncology letters. 2019 Dec;18(6):5673-80.
82. Bansal K, Balaji KN. Intracellular pathogen sensor NOD2 programs macrophages to trigger Notch1 activation. Journal of Biological Chemistry. 2011 Feb 18;286(7):5823-35.
83. Zhao L, Lee JY, Hwang DH. The phosphatidylinositol 3-kinase/Akt pathway negatively regulates Nod2-mediated NF-κB pathway. Biochemical pharmacology. 2008 Apr 1;75(7):1515-25.
84. Fuentes N, Silveyra P. Estrogen receptor signaling mechanisms. Advances in protein chemistry and structural biology. 2019 Jan 1;116:135-70.
85. Cotrim CZ, Fabris V, Doria ML, Lindberg K, Gustafsson JÅ, Amado F, Lanari C, Helguero LA. Estrogen receptor beta growth-inhibitory effects are repressed through activation of MAPK and PI3K signalling in mammary epithelial and breast cancer cells. Oncogene. 2013 May;32(19):2390-402.
86. Ghayad SE, Vendrell JA, Larbi SB, Dumontet C, Bieche I, Cohen PA. Endocrine resistance associated with activated ErbB system in breast cancer cells is reversed by inhibiting MAPK or PI3K/Akt signaling pathways. International journal of cancer. 2010 Jan 15;126(2):545-62
87. Gupta N, Bostrom AG, Kirschner BS, Ferry GD, Winter HS, Baldassano RN, Gold BD, Abramson O, Smith T, Cohen SA, Heyman MB. Gender differences in presentation and course of disease in pediatric patients with Crohn disease. Pediatrics. 2007 Dec 1;120(6):e1418-25.
88. Greuter T, Manser C, Pittet V, Vavricka SR, Biedermann L. Gender differences in inflammatory bowel disease. Digestion. 2020 Sep 29;101(Suppl. 1):98-104.
89. Moktan VP, Daoud ND, Tremaine WJ, Loftus Jr EV, Kane SV, Hochwald AP, Hodge DO, Hashash JG, Faubion SS, Farraye FA. A cohort study of the age at menopause in female patients with and without inflammatory bowel disease. Crohn's & Colitis 360. 2022 Jul 1;4(3):otac027.
90. Kane SV, Reddy D. Hormonal replacement therapy after menopause is protective of disease activity in women with inflammatory bowel disease. Official journal of the American College of Gastroenterology| ACG. 2008 May 1;103(5):1193-6.
91. Freeman M, Lally L, Teigen L, Graziano E, Shivashankar R, Shmidt E. Hormone Replacement Therapy Is Associated with Disease Activity Improvement among Post-Menopausal Women with Inflammatory Bowel Disease. Journal of Clinical Medicine. 2023 Dec 23;13(1):88.
92. Andreoli L, Guadagni I, Picarelli G, Principi M. Comprehensive reproductive healthcare for women with immune-mediated inflammatory diseases: Addressing rheumatoid arthritis, spondyloarthritis and inflammatory bowel disease through life's stages. Autoimmunity Reviews. 2024 Mar 1;23(3):103507.
93. Severs M, Spekhorst LM, Mangen MJ, Dijkstra G, Löwenberg M, Hoentjen F, van der Meulen-de Jong AE, Pierik M, Ponsioen CY, Bouma G, Van Der Woude JC. Sex-related differences in patients with inflammatory bowel disease: results of 2 prospective cohort studies. Inflammatory bowel diseases. 2018 May 18;24(6):1298-306.
94. Lungaro L, Costanzini A, Manza F, Barbalinardo M, Gentili D, Guarino M, Caputo F, Zoli G, De Giorgio R, Caio G. Impact of female gender in inflammatory bowel diseases: a narrative review. Journal of personalized medicine. 2023 Jan 17;13(2):165.
95. Kane SV, Sable K, Hanauer SB. The menstrual cycle and its effect on inflammatory bowel disease and irritable bowel syndrome: a prevalence study. The American journal of gastroenterology. 1998 Oct 1;93(10):1867-72.

96. Whitehead WE, Cheskin LJ, Heller BR, Robinson JC, Crowell MD, Benjamin C, Schuster MM. Evidence for exacerbation of irritable bowel syndrome during menses. Gastroenterology. 1990 Jun 1;98(6):1485-9.
97. Adeyemo MA, Spiegel BM, Chang L. Meta-analysis: do irritable bowel syndrome symptoms vary between men and women?. Alimentary pharmacology & therapeutics. 2010 Sep;32(6):738-55.
98. Saha S, Zhao YQ, Shah SA, Esposti SD, Lidofsky S, Salih S, Bright R, Law M, Moniz H, Flowers N, Merrick M. Menstrual cycle changes in women with inflammatory bowel disease: a study from the ocean state Crohn's and colitis area registry. Inflammatory bowel diseases. 2014 Mar 1;20(3):534-40.